7-21-2008

Experimental characterization of Cr4+:YAG passively Q-switched Cr:Nd:GSGG lasers and comparison with a simple rate equation model

Nathan Longbotham

Follow this and additional works at: https://digitalrepository.unm.edu/ose_etds

Experimental Characterization of Cr^{4+}:YAG Passively Q-switched Cr:Nd:GSGG Lasers and Comparison with a Simple Rate Equation Model

by

Nathan W. Longbotham

B.S., Physics, Abilene Christian University, 2001

THESIS

Submitted in Partial Fulfillment of the
Requirements for the Degree of

Master of Science
Optical Science and Engineering

The University of New Mexico

Albuquerque, New Mexico

May, 2008

Experimental Characterization of Cr^{4+}:YAG Passively Q-switched Cr:Nd:GSGG Lasers and Comparison with a Simple Rate Equation Model

by

Nathan W. Longbotham

ABSTRACT OF THESIS

Submitted in Partial Fulfillment of the
Requirements for the Degree of

Master of Science
Optical Science and Engineering

The University of New Mexico

Albuquerque, New Mexico

May, 2008

Experimental Characterization of Cr^{4+}:YAG Passively Q-switched Cr:Nd:GSGG Lasers and Comparison with a Simple Rate Equation Model

by

Nathan W. Longbotham

B.S., Physics, Abilene Christian University, 2001

M.S., Optical Science and Engineering, University of New Mexico, 2008

Abstract

This thesis presents a study on the comparison and anlysis of a laser rate equation model and the laboratory performance of passively Q-switched microlasers. The laser rate equation model describes the development of a top hat gain distribution taking into account the excited state absorption of the passive Q-switch. The lasers examined are Cr:Nd:GSGG lasers passively Q-switched by a Cr^{4+}:YAG crystal. This work will focus on the performance of these lasers as a function of two key design parameters, the passive Q-switch initial transmission (T_0) and laser resonator output coupling (R_{OC}), when values are varied over a wide range. Four lasers, each with unique T_0 and R_{OC} values, are studied. Characterization of each laser consists of measuring the energy fluence and duration of the laser pulses. The agreement of these measurements with the calculated values is then analyzed in order to understand

the maximum deviation that can be expected from lasers constructed using the simple rate equation model as a design tool. The presented analysis shows that laser pulse fluence measurements deviate from the rate equation model calculations by a maximum of 30% across all measured lasers and that the data fits well to the rate equation calculated fluence values. The agreement of the calculated pulse duration estimates with the experimental data is less successful. The measured data deviates from the calculated values by as much as 90% . The rate equation model consistently overestimates the laser pulse duration, and it does increasingly so for lasers designed with lower R_{OC} and larger T_0 values. The data presented shows that a simple rate equation model to be used as a laser design tool is useful in developing preliminary designs for low-order transverse mode lasers. However, care should be exercised when a precise understanding of the laser pulse duration is required.

Contents

Contents

List of Figures

x

List of Tables

Glossary

Cr:Nd:GSGG   Chromium and Neodymium doped Gadolinium Scandium Gallium Garnet, the gain medium used in this thesis.

Cr^{4+}:YAG   Chromium^{4+} doped Yttrium Aluminum Garnet, the saturable absorber Q-switch material used in this thesis.

R_{OC} Laser resonator output coupler reflectivity.

T_0 Saturable absorber Q-switch initial transmission.

Chapter 1

Introduction

With the development of passively Q-switched laser systems and solid state laser materials, small high power lasers have became much more practical for a variety of applications. The solid state materials that compose many modern passively Q-switched lasers are thermally and mechanically robust. These materials, combined with diode laser pump systems, enable compact passively Q-switched laser systems to be engineered. They are capable of producing high power, short pulse durations, excellent beam quality, and operate at relatively high efficiencies. Because of these favorable properties, they have enabled new capabilities for many technologies, including nonlinear optics, range finding, and remote sensing.

In order for these devices to be appropriately designed for a given application, it is necessary to have models capable of accurately predicting the output characteristics of these lasers. As solid state passively Q-switched lasers were developed, so were models capable of describing them. The standard approach for analyzing the performance of passively Q-switched lasers is to solve the rate equations. These equations are based on the evolution of atomic population densities in the laser and Q-switch materials.

These rate equation models have been widely discussed in literature. Soon after the first laser was operated in 1960, giant optical pulses began to be discussed and experimentally validated.[1–4] Early publications also described the differential equations that govern the population inversion and photon density in Q-switched lasers.[5–7] With advance of passively Q-switch devices, renewed attention was given to rate equation development for these devices. Degnan [8] originally derived key performance parameters of passively Q-switched laser describing energy, power, and pulse duration. Additional rate equation treatments were published providing methodologies for optimizing performance of passively Q-switched systems.[9, 10] Others extended this approach to account for excited state absorption of passive Q-switches in which residual loss remains during the laser pulse development, as is that case in many solid state Q-switches.[11–14]

Throughout the development of the Q-switched rate equation models, experimental verifications of the model calculations have been reported.[13–16] However, these investigations were performed for a single set of laser design parameters. In order to provide an understanding of a simple rate equation model's applicability to sensitivity studies, the current work seeks to extended verification of a simple rate equation model to multiple lasers that span the range of fundamental passively Q-switched laser design parameters. The central design parameters studied in this thesis are the Q-switch initial transmission (T_0) and the laser output coupling reflectivity (R_{OC}). The study is carried out using Cr:Nd:GSGG lasers passively Q-switch with Cr^{4+}:YAG. The simple rate equation model chosen to calculate the laser output characteristics in this thesis was developed by Zhang *et al.* ([11]).

1.1 Thesis Objectives

The work presented in this thesis is designed to quantitatively understand practical limitations of the rate equation model as it describes a Cr:Nd:GSGG laser passively Q-switched by a Cr^{4+}:YAG crystal. The work will experimentally analyze the rate equation model calculated laser performance values for several microlasers designed with a variety of initial Q-switch transmission (T_0) and laser output mirror reflectivity (R_{OC}) values. In order to accomplish this, three goals are identified:

1. Develop laser performance calculations from a plane wave rate equation model that describes Cr:Nd:GSGG, Cr^{4+}:YAG passively Q-switched lasers.

2. Assemble Cr:Nd:GSGG, Cr^{4+}:YAG passively Q-switched lasers with various T_0 and R_{OC} values and measure the Q-switched laser fluence and pulse duration.

3. Compare the rate equation model calculations to the laboratory performance of the measured laser systems and characterize the correlation.

1.2 Q-switching Process

Q-switching is a method of manipulating a laser system such that it produces a short, high energy laser pulse. It is named for the switching of the laser cavity quality factor (Q). In a Q-switched laser, the loss of the cavity is temporarily increased (and therefore the cavity quality factor is decreased), preventing oscillation of the laser and creating excess gain in the cavity. By allowing the laser gain to increase beyond what it would be in the absence of the temporary loss, and then switching the resonator quality to a high value, the excess gain is released in a short, high energy laser pulse.

Figure 1.1 illustrates the interrelationship of the laser gain, laser loss, and the accompanying output pulse in a Q-switching laser. With the cavity loss initially high, the gain increases to levels well above what would be accumulated absent the temporary loss. When the quality is switched high again, the stored gain inversion is quickly released to the laser oscillation creating an exponential increase in the intracavity photon density, and consequently, the output laser pulse. The photon density increases until the population inversion is reduced to the point at which the laser would come to threshold with the lower loss level (n_t). After the point of peak photon density, the output pulse decreases to the point at which the available gain is depleted by the laser pulse.
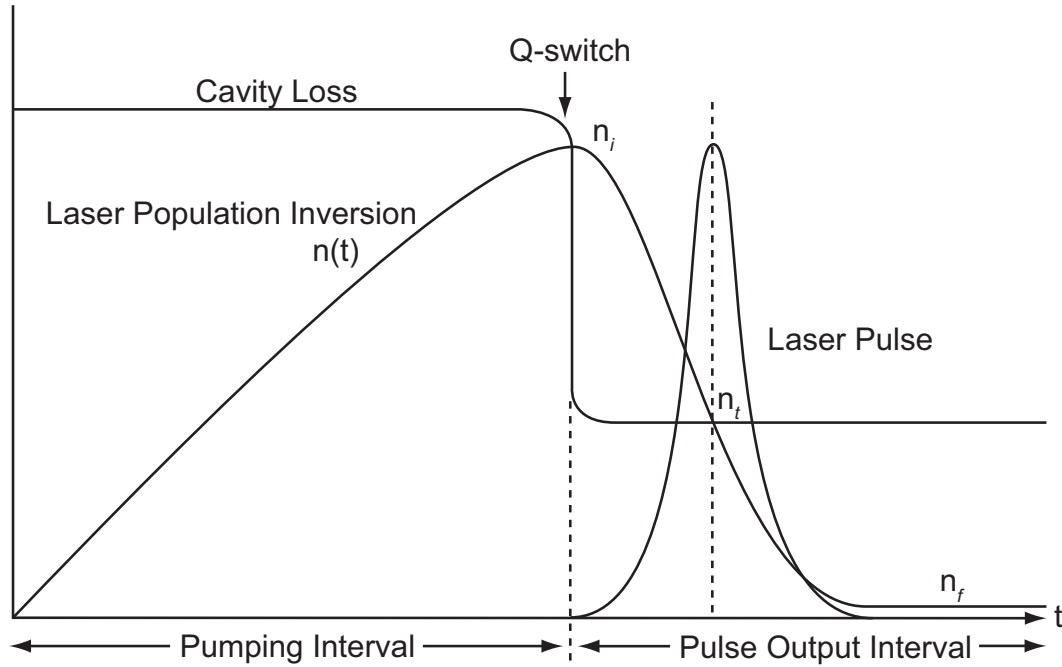
Figure 1.1: Time evolution of the gain, loss, and output pulse in a Q-switched laser. The initial population inversion (n_i) at the onset of Q-switching is reduced at the expense of the increasing photon density until the population inversion of the laser would come to threshold with the lower loss level (n_t). From this point of peak power, the photon density depletes the population inversion to a final value (n_f), determined by the ratio of n_i/n_t.[17–19]

The initial population inversion (n_i) is the population inversion of the laser medium at the onset of Q-switching. The specific value is determined by the level of temporary loss induced by the Q-switching process. It is also subject to an upper limit determined by energy loss due to spontaneous emission out of the upper energy level of the laser medium. This also causes additional loss when the spontaneous emission is amplified by the population inversion. These effects create a limit to the amount of energy that can be stored in the laser population inversion.

The population inversion at maximum photon density (n_t) is determined by the lower loss level of the Q-switching process. The photon density increases from the onset of the Q-switch and peaks at the point which the gain from the population inversion would come to threshold with the lower loss level.

The level of final population inversion depletion (n_f) is a function of the population inversion at the time of Q-switch initiation (n_i) and at peak power (n_t). The ratio of the two values (n_i/n_t) determines the amount of population inversion depletion. If n_i is close to the population at the lasing threshold in the absence of a Q-switch (n_t), then n_f will be depleted approximately an amount below n_t as n_i is above it. However, if n_i is much larger than n_t, then the Q-switch pulse will completely deplete the population inversion such that n_f is approximately zero.[17–19]

1.3   Q-switching Mechanisms

There are four types of mechanisms that provide Q-switching action: mechanical, electro-optic, acousto-optic, and passive absorption. Q-switch mechanisms of the mechanical, electro-optic, and acousto-optic types are considered active Q-switches. These rely on input from outside of the laser cavity to trigger the Q-switching mechanism. In contract, passive Q-switches rely on the energy build-up inside the cavity to trigger the Q-switching action. As an introduction, both types are discussed below,

but the presentation in this thesis is focused on passively Q-switched lasers.

1.3.1 Active Q-switches

Mechanical Q-switches have often been used in Q-switching applications due to their simplicity. Most of these devices inhibited laser action through the use of rotating mirrors or choppers placed in the laser resonator. These relatively simple mechanisms provided excellent Q-switching because they induce full loss at low Q, but also reduce to full transmittance at high Q. However, they have mostly been replaced by electro-optic and acousto-optic devices due to their relatively slow Q-switching process.

Some of the earliest examples of Q-switching employed the use of an electro-optic modulator.[2, 4] These devices takes advantage of a strong electro-optic property exhibited by some materials through which they become birefringent under the influence of an external electric field. At the expense of added complexity in the necessary electronics to drive the applied electric field, these devices provide very fast Q-switching action - limited by the ability to switch the applied voltage. The most popular examples of these devices are the Pockels and Kerr cells. The difference between the two being that the birefringence in the materials used for a Kerr cell responds to the square of the applied electric field, while the Pockels cell is linearly dependent. Pockels cells are usually preferred because of the higher voltages necessary to induce polarization rotation and the volatile nature of nitrobenzene, the typical material employed in Kerr cells.

Figure 1.2 shows a representation of a typical elctro-optic Q-switch setup. Utilizing the induced birefringence, linearly polarized radiation propagating through the Kerr cell can be rotated. By carefully using this property, the loss of a laser resonator can be temporarily increased by coupling the intracavity radiation out of the cavity, creating a low quality resonator (Figure 1.2(a)). When sufficient energy is

accumulated in the laser material, the linearly polarized light produced by the laser (shown in Figure 1.2 as polarized in the plane of the table) is rotated 90° in the Kerr cell. This change in the Kerr cell switches the loss low and allows the laser to oscillate (Figure 1.2(b)).

(a)

(b)
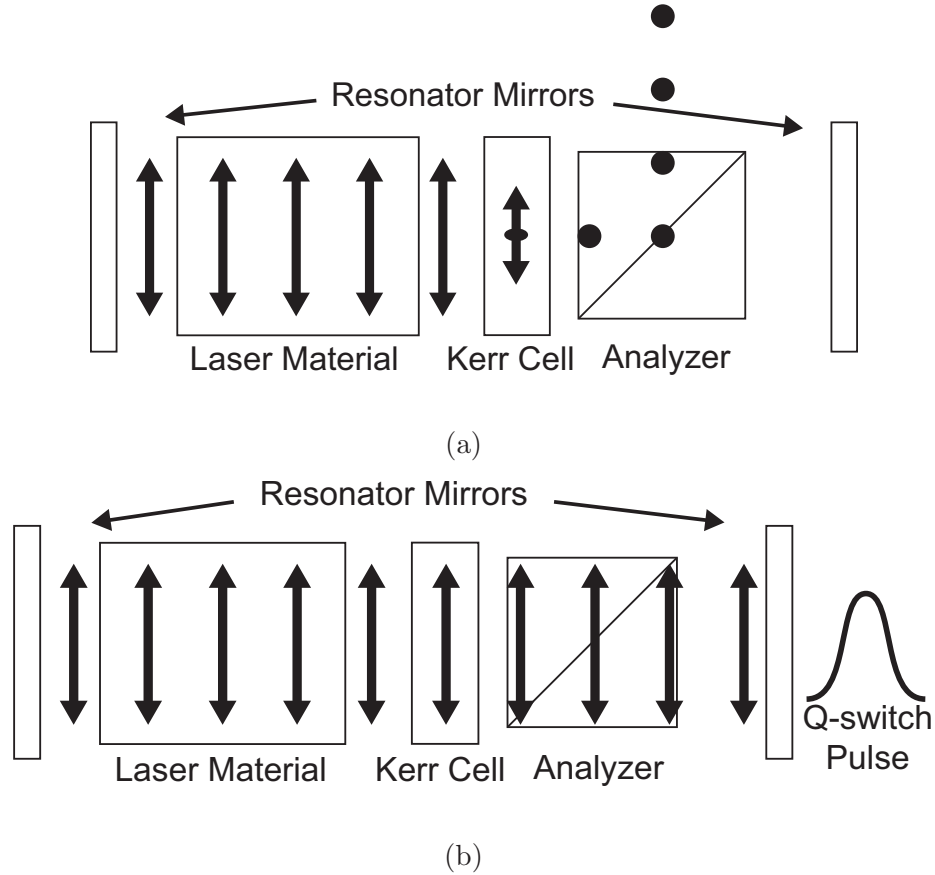
Figure 1.2: Utilizing electrically induced birefringence in a Kerr cell, laser oscillation is held off by manipulating the orientation of linearly polarized laser radiation and selectively coupling it out of the cavity through an optical analyzer. Laser oscillation is held off while the cavity quality is low and radiation is coupled out of the cavity(a). Q-switching is achieved by removing the cavity loss and allowing laser radiation(b).[17, 20]

Acousto-optic modulators utilize the property of photoelasticity, or a change in the refractive index of a material due to mechanical stress. By inducing periodic

mechanical stress on a crystal, through the use of an acoustic wave, a period change in the index of refraction is created through the crystal. As illustrated in Figure 1.3, this causes the crystal to act as a diffraction grating, diffracting part of the beam out of the normal resonator path. When the acoustic field is turned off, the Q-switch allows the beam to propagate normally, yielding a high quality resonator state. The Q-switch speed is slower than an electro-optic Q-switch, limited by the propagation speed of the acoustic wave across the crystal and the beam diameter. However, the availability of high optical-quality materials for this application produces a device with very low optical loss.[17, 20]
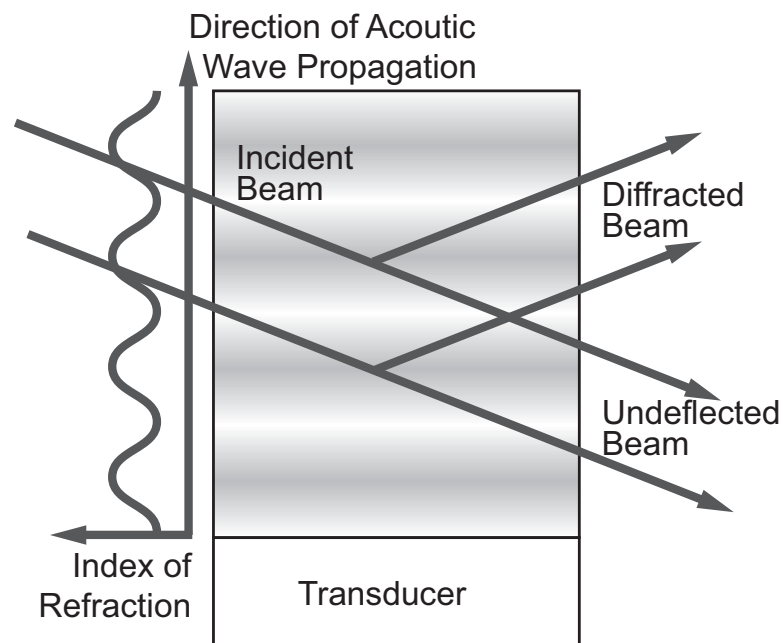
Figure 1.3: An acousto-optic Q-switch creates loss by inducing acoustic stress waves across a crystal. This induced strain causes variation, with frequency and amplitude determined by the applied acoustic wave, in the index of refraction across the crystal. This causes the material to act as a diffraction grating and to diffract a portion of the incident laser beam out of the laser cavity. High resonator quality is returned when the acoustic wave is removed.[17, 20]

1.3.2   Passive Q-switches

A passive Q-switch is a mechanism that changes the loss of a laser resonator in response to the internal photon density of the laser. Since the laser itself triggers the Q-switch action, there is no high voltage, timing electronics, acoustic transducer, or other complexities necessary for the Q-switch process. This allows for very simple and compact construction of high power pulsed lasers.

This is a significant advantage, but because the system self-triggers, there are additional complexities. Because there is no external trigger, the system lacks the ability to externally determine the timing of the Q-switched pulse. This ambiguity must be addressed in cases where laser timing is essential to composite system operation. In addition, sequential pulses from a passively Q-switched laser will show some temporal deviation from a perfectly periodic pulse train. This variation is referred to as timing jitter. In passively Q-switched systems, this is due to fluctuations in the pump power and residual energy in the gain material. There are methods to control the timing jitter [21, 22], but care must be taken when using passively Q-switched systems for applications that require precise timing. Despite these limitations, the simplicity of passively Q-switched systems makes them an acceptable trade off for many applications.

Although alternative passive methodologies have been reported, such as thin film Q-switches that use ablation of a substance in response to photon density inside the laser, to provide the Q-switch mechanism [23, 24], most passive Q-switches employ a saturable absorber material. These materials use an absorption transition at the laser wavelength to induce loss in the laser resonator. These materials will initially prevent laser oscillation due to their ability or absorb energy at the laser wavelength. If the lifetime of this absorption transition is long enough that the photon density in the cavity is able to saturated the transition, the initial cavity loss is reduced

and will eventually allow the cavity to oscillate. This is discussed in more detail in Section 1.4.3.

Originally, saturable absorbers were based on organic dyes. These were difficult to work with and suffered from high degradation rates. Because of these issues, the most common passive Q-switches are now solid state saturable absorbers, such as Cr^{4+}:YAG. These solid state passive Q-switches are robust when compared to alternative passive Q-switching materials, making them well suited for construction of small, high energy lasers.

Saturable absorber materials also exhibit residual absorption that adds loss to the lasing action after the Q-switch has been switched to a high quality state. This is due to secondary absorption transitions at the laser wavelength that can not be saturated. The properties of excited state absorption for the passive Q-switch material used in this thesis, Cr^{4+}:YAG, will be discussed further in Section 1.4.3.[17, 19]

1.4 Laser Resonator and Materials

While a more specific discussion of the lasers analyzed in this thesis will be presented in Chapter 3, Figure 1.4 illustrates the basic elements of the solid state passively Q-switched lasers to be analyzed. These elements include the resonator mirrors, a gain medium, and a passive Q-switch.

1.4.1 Laser Resonator

The laser resonator to be used in this work is comprised of two flat mirrors. The input mirror is a high reflector at the laser wavelength and anti-reflective at the pump wavelength to allow the laser to be end-pumped via a fiber coupled laser diode. The

Figure 1.4: Illustration of the basic components of the passively Q-switched lasers studied in this thesis. The laser consists of Cr:Nd:GSGG gain material followed by a Cr^{4+}:YAG passive Q-switch. The input and output mirrors are coated directly onto the resonator crystals, creating a flat-flat resonator. The laser resonator is end-pumped by a laser diode at 808 nm and produces a Q-switched laser pulse at 1061 nm.

output mirror is a partial reflector at the laser wavelength. The exact value of the partial reflectivity (R_{OC}) varies from laser to laser and is one of two key design parameters that determine the output energy. The second key design parameter, Q-switch initial transmission (T_0), is discussed in Section 1.4.3.

End pumping the laser resonator provides several design advantages. Most importantly, it is an efficient design. The pumped region of the laser medium can overlap the TEM_{00} laser mode which allows the stored energy to be optimally transferred to the low-order laser mode. Higher order laser modes will not oscillate because they will not have sufficient gain. The end-pumped arrangement also provides good flexibility when engineering the physical arrangement of the laser resonator and pump systems because the two can be treated as separate packages that need only be connected by an optical fiber.

The disadvantage of end pumping is that it also imparts thermal gradients to the laser rod. Since more of the energy introduced to the laser rod is absorbed near the input mirror, there is a energy distribution induced near the input mirror along the longitudinal axis of the laser rod as well as a radial variation due to the Gaussian

shape of the laser pump energy. Through the processes of quantum defect heating and nonradiative relaxation, this absorbed laser energy creates a thermal gradient in the laser rod near the end that is absorbing the pump energy.

At higher laser power levels, this thermal energy must be managed to prevent fracture of the laser rod due to the physical stresses induced by the thermal gradients. At the lower power levels used in this thesis, the effect of interest is the accompanying thermal lensing. The variation in the absorbed laser pump energy induces thermal gradients near the input mirror of the laser. The change in thermal energy in the laser rod alters the index of refraction and causes lensing in the laser rod that slightly alters the resonator stability. This lensing can be conceptualized as an additional concave curvature of the input mirror. The induced curvature of the input mirror makes the precise resonator configuration a function of the pump laser's power and beam diameter. This effect is not modeled as part of the rate equation model because the simple plane wave assumption bears no dependency on radial variations in the laser rod (see Section 2.1).[17]

1.4.2 Laser Gain Material

The laser gain material used in this thesis is Chromium and Neodymium co-doped Gadolinium Scandium Gallium Garnet (Cr:Nd:GSGG). Cr:Nd:GSGG is a specialty laser material that was originally developed as a means to improve flashlamp absorption of the laser material. This was achieved by co-doping Cr ions into the Nd:GSGG laser host and taking advantage of the broad absorption bands of the Cr ions. In GSGG, the Cr ions are able to transfer nearly 100% of their absorbed energy to the Nd laser transition energy level.[25–27]

Cr:Nd:GSGG also has many optical and mechanical properties that are useful in non-flashlamp pumped Q-switched lasers. It is stable, optically isotropic, and is

resistant to radiation induced damage. It is similar in many ways to the Nd:YAG laser material, with the exception of lower values for thermal conductivity and stimulated emission cross section. The lower thermal conductivity is not of significant concern in low duty cycle lasers. However, the reduced stimulated emission cross section is useful because it reduces amplified spontaneous emission (ASE), allowing more energy to be stored in a gain medium before the parasitic effect of ASE becomes significant. This means the laser material provides better Q-switching efficiency and potentially higher extracted energy.[28–30] For a detailed discussion of Cr:Nd:GSGG as a laser material, please see Koechner [31].

1.4.3 Laser Q-switch Material

Chromium[4+] doped Yttrium Aluminum Garnet (Cr^{4+}:YAG) is used as the passive Q-switch material for the lasers analyzed in this thesis. It is a popular passive Q-switch because it has favorable thermal and mechanical properties. It also has a much higher damage threshold than the organic based passive Q-switches that were common prior to the development of solid state varieties. The material also has a strong absorption cross section near the laser transition of Cr:Nd:GSGG at λ=1061 nm.[32–35]

The energy levels of the Cr^{4+}:YAG passive Q-switch can be modeled as a four level system. There is some disagreement on the exact structure of the energy levels involved in the saturable absorption process.[36] However, the rate equation model does not depend on the details of the energy level diagram. It is modeled such that there is ground state saturable absorption and excited state non-saturable absorption, as is the case in Cr^{4+}:YAG.[35, 37–39] A simplified energy level diagram showing the transitions important to passive Q-switching in Cr^{4+}:YAG is given in Figure 1.5.

The 1-3 transition is the targeted saturable transition. When a photon at the
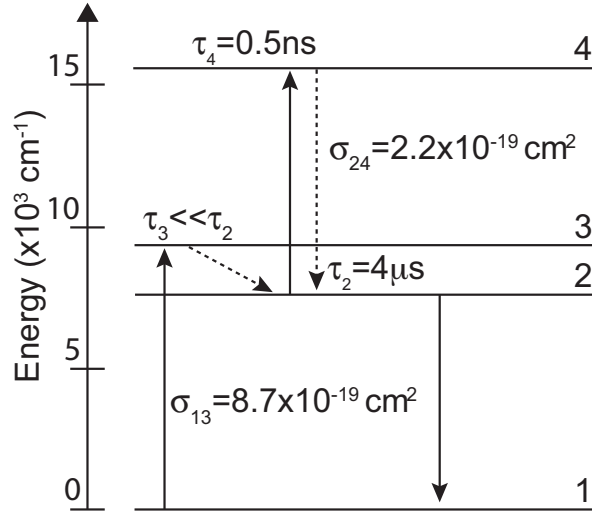
Figure 1.5: A four level energy diagram of a Cr^{4+}:YAG passive Q-switch. The transitions applicable to passive Q-switching are shown. Energy absorbed by the ground state transition (1-3) immediately relaxes into level 2. This energy level has a long lifetime, allowing the Q-switch to become saturated. The excited state absorption transition (2-4) has a very short lifetime (and thus does not saturate) and induces appreciable loss in the saturated Q-switch which must be accounted for in rate equation models.[40–42]

laser wavelength is absorbed by the ground state, energy level 3 immediately relaxes to level 2. This level has a long lifetime (τ_2=4 μs), allowing the 1-3 transition to become saturated as the population of level 1 is depleted. In contrast, energy level 4 has a very short lifetime (τ_4=0.5 ns) such that there is no appreciable population in this level. Because of this, the 2-4 transition does not saturate. However, it does add significant loss to the resonator during the production of the Q-switch pulse, referred to as excited state absorption. This effect becomes more pronounced as the Q-switch becomes saturated and more population is available in level 2. Therefore, it is important that this effect is included in any rate-equation model that describes a passive Q-switch.[11, 12, 17, 43]

The second key design parameter of the lasers used in this thesis, the initial transmission of the saturable absorber (T_0), arises from the ground state absorption

of the Q-switch. It is the small signal transmission of the Q-switch, and can be thought of as the Q-switch hold-off loss. The specific value of T_0 for a passive Q-switch is a function of the material cross section (σ_{13}=8.7x10^{-19} cm^2 for Cr^{4+}:YAG) as well as the length of the saturable absorber.[11, 17, 36]

Chapter 2

Rate Equation Model

To aid in the design of passively Q-switched lasers, rate equation models that are based on the evolution of atomic population densities in Q-switch materials have been developed.[5, 8] As passively Q-switched lasers have progressed to using solid state materials, the rate equations have been modified to more accurately model excited state absorption that is associated with these materials.[11, 12] The following chapter is a brief introduction to the rate equation model that is used in this thesis to describe solid state Cr:Nd:GSGG, Cr^{4+}:YAG passively Q-switched lasers.

2.1   Rate Equations and Solutions

The following presentation of the rate equations was developed by Zhang *et al.* ([11]). This specific rate equation model was chosen because it provides accurate and accessible calculations for the design of Cr^{4+}:YAG passively Q-switched lasers. It includes saturable absorber excited state absorption effects of Cr^{4+}-doped crystals, but keeps the calculations involved in solving the rate equations relatively simple by assuming a top-hat gain distribution that is uniformly distributed throughout the gain medium,

as opposed to a more complex Gaussian distribution [15].

Equations 2.1, 2.2, and 2.3 are the coupled rate equations, as reported in Zhang [11], that describe the evolution of a single passively Q-switched laser pulse modified to include excited state absorption by using a four level Q-switch model. These three equations describe the time rate of change of the cavity photon density (ϕ), laser population inversion density (n), and the population density in the lower atomic level of the Q-switch (n_{s1}).

$$\frac{d\phi}{dt} = \frac{\phi}{t_r}\left[2\sigma n l - 2\sigma_{13}n_{s1}l_s - 2\sigma_{24}(n_{s0} - n_{s1})l_s - \ln\left(\frac{1}{R}\right) - L\right] \quad (2.1)$$

$$\frac{dn}{dt} = -\gamma\sigma c\phi n \quad (2.2)$$

$$\frac{dn_{s1}}{dt} = -\sigma_{13}c\phi n_{s1} \quad (2.3)$$

Equation 2.1 is the mathematical description of the time varying resonator photon density. This description includes various mechanisms contributing to the cavity photon density. $2\sigma n l$ is the gain of the laser material. The terms $2\sigma_{13}n_{s1}l_s$ and $2\sigma_{24}(n_{s0} - n_{s1})l_s$ express the loss of photon density as a result of the absorbing atomic transitions of the Q-switch ground state and excited state respectively over the length of the saturable absorber (l_s). The remaining two contributions are also losses in the cavity. The first, $\ln(\frac{1}{R})$, is the useful loss due to output coupling of the laser beam from the cavity. The second, L, is the remaining loss due to other cavity processes, such as material scattering.

Equation 2.2 describes the population inversion of the laser gain material through stimulated emission. It describes the negative rate of change of the laser population inversion density (dn/dt) due to higher population inversion (n) and photon flux (ϕ) in the laser.

ϕ	Photon flux in the cavity
σ	Laser stimulated emission cross section
σ_{13}	Q-switch absorption cross section of the 1-3 atomic transition
σ_{24}	Q-switch absorption cross section of the 2-4 atomic transition
n	Instantaneous laser population inversion density
n_{s1}	Instantaneous Q-switch population density in level 1
n_{s2}	Instantaneous Q-switch population density in level 2
n_{s0}	Total Q-switch population density $(n_{s1}+n_{s2})$
l	Length of the laser medium
l_s	Length of the saturable absorber
t_r	Round-trip transit time of light in the cavity
l'	Optical length of the laser resonator
R	Reflectivity of the laser cavity output mirror
T_0	Initial transmission of the saturable absorber
L	Total round trip cavity loss not accounted for by other parameters
γ	Laser inversion reduction factor
c	Speed of light in a vacuum
hν	Photon energy
A	Active area of the beam in the laser material
α	Q-switch absorption and laser emission cross section ratio
n_i	Laser population inversion density at $t = 0$
n_f	Laser population inversion density after the laser pulse
n_t	Laser population inversion density at point of peak power
n_{t0}	n_t when α approaches infinity

Table 2.1: Rate equation model input parameters.

Similarly, Equation 2.3 describes the change in population density of the Q-switch ground state, the saturable transition. It describes the negative rate of change of the Q-switch ground state population density (n_{s1}) due to excitation of the n_{s1} population by increasing photon density (ϕ) in the laser and the resulting reduction of the n_{s1} population.

In the above equations, γ is the inversion reduction factor. It describes the change in laser population inversion when the population of the excited state is decreased by one. For a four level laser (as is the case with a Cr:Nd:GSGG laser), γ is one. If the rate equations were modeling a three level laser, γ would be two because

the creation of a stimulated photon would also increase the population of the laser medium ground level by one and effectively reduce the laser population inversion by two.

This rate equation model is a plane wave model that assumes a uniform population inversion in the gain medium, and therefore a uniform beam profile in the laser. It neglects the transverse mode volume of Q-switched lasers and assumes all energy in a cylindrical volume of the gain medium contributes to the beam output. Because of this, it is possible that the laboratory measurement of laser resonator Gaussian transverse modes could produce a systematic offset from the rate equation model fluence description. In order to minimize this source of error, in this thesis data is collected only from TEM$_{00}$ laser modes. The presence of multimode lasing could produce significantly different results from this study and alter the applicability of the presented rate equation model.

This set of rate equations neglects both continued laser pumping and spontaneous emission. This assumption is made because of the fast nature of the Q-switching process. This means that the change in population inversion due to laser pumping and spontaneous emission is small enough that there is a negligibly small change during the time it takes the Q-switch pulse to be produced. These assumptions can affect some results of the rate equation model, such as the estimation of necessary pump energy, but do not contribute to the calculated properties of the laser pulse studied in this thesis.

Two additional parameters are used in the rate equation solutions to describe the interaction of the passive Q-switch and laser medium. These variables of interest are δ and α [11]:

$$\delta = \frac{\sigma_{24}}{\sigma_{13}} \tag{2.4}$$

$$\alpha = \frac{\sigma_{13}}{\gamma\sigma} \tag{2.5}$$

δ describes the relative strength of the two absorption cross sections, the ground state (σ_{13}) and the excited state (σ_{24}), in the saturable absorber Q-switch. It gives a quantitative description of the probability that a photon at the laser wavelength will be absorbed in either of the atomic transitions. The second variable, α, describes the relative strength of the absorption transitions of the laser and Q-switch mediums.

Using the parameter α, we can describe the relationship between the Q-switch total population density (n_{s0}) and population density in the atomic level one of the Q-switch (n_{s1}). This is done by dividing Equation 2.2 by 2.3 and integrating the result to produce:

$$\frac{n_{s1}}{n_{s0}} = \left(\frac{n}{n_i}\right)^{\alpha} \tag{2.6}$$

The above equations allow us to derive descriptions of the photon flux with a dependence on n. By dividing the equations describing $d\phi/dt$ and dn/dt (Equations 2.1 and 2.2) and substituting Equations 2.4, 2.6, and $2\sigma n_{s0}l_s = \ln\left(1/T_0^2\right)$, we eliminate the time dependence of the laser photon flux and describe the change in photon flux as a function of the population inversion [11]:

$$\frac{d\phi}{dn} = \frac{-l}{\gamma l'}\left[1 - \frac{(1-\delta)\ln\left(\frac{1}{T_0^2}\right)}{2\sigma nl}\left(\frac{n}{n_i}\right)^{\alpha} - \frac{\ln\left(\frac{1}{R}\right) + \delta\ln\left(\frac{1}{T_0^2}\right) + L}{2\sigma nl}\right] \tag{2.7}$$

Integrating this equation yields:

$$\begin{aligned}
\phi(n) \;=\; &\frac{l}{\gamma l'}\left[n_i - n - \frac{\ln\left(\frac{1}{R}\right) + \delta\ln\left(\frac{1}{T_0^2}\right) + L}{2\sigma l}\ln\left(\frac{n_i}{n}\right)\right.\\[2mm]
&\left. - \frac{(1-\delta)\ln\left(\frac{1}{T_0^2}\right)}{2\sigma l}\frac{1}{\alpha}\left(1 - \frac{n^{\alpha}}{n_i^{\alpha}}\right)\right]
\end{aligned} \tag{2.8}$$

Equations 2.7 and 2.8, along with Equation 2.1, allow us to create descriptions of the initial populations inversion (n_i), the population inversion at peak power (n_t), and the final population inversion (n_f) as a function of fundamental material properties of the laser. By setting Equation 2.1 equal to zero and using the fact that $n_{s1}(t = 0) = n_{s0}$, we can express the population inversion at Q-switch threshold:

$$n_i = \frac{\ln\left(\frac{1}{R}\right) + 2\sigma_{13} n_{s0} l_s + L}{2\sigma l} \tag{2.9}$$

Setting Equation 2.7 equal to zero we can obtain an expression describing the population inversion at the point of maximum power:

$$\frac{n_t}{n_i} = \frac{\ln\left(\frac{1}{R}\right) + \delta \ln\left(\frac{1}{T_0^2}\right) + L}{2\sigma n_i l} + \frac{(1-\delta)\ln\left(\frac{1}{T_0^2}\right)}{2\sigma n_i l}\left(\frac{n_t}{n_i}\right)^\alpha \tag{2.10}$$

Similarly, setting Equation 2.8 equal to zero we can obtain an expression describing the final population inversion density:

$$n_i - n_f \quad - \quad \frac{\ln\left(\frac{1}{R}\right) + \delta \ln\left(\frac{1}{T_0^2}\right) + L}{2\sigma l} \ln\left(\frac{n_i}{n_f}\right)$$
$$- \quad \frac{(1-\delta)\ln\left(\frac{1}{T_0^2}\right)}{2\sigma l}\frac{1}{\alpha}\left[1 - \left(\frac{n_f}{n_i}\right)^\alpha\right] = 0 \tag{2.11}$$

Creating a new parameter, n_{t0}:

$$n_{t0} = \frac{\ln\left(\frac{1}{R}\right) + \delta \ln\left(\frac{1}{T_0^2}\right) + L}{2\sigma l} \tag{2.12}$$

we can simplify Equations 2.10 and 2.11 into two transcendental equations that describe the relationship between n_t/n_i and n_f/n_i [11]:

$$\frac{n_t}{n_i} = \frac{n_{t0}}{n_i} + \left(1 - \frac{n_{t0}}{n_i}\right)\left(\frac{n_t}{n_i}\right)^\alpha \tag{2.13}$$

$$1 - \frac{n_f}{n_i} + \left(\frac{n_{t0}}{n_i}\right)\ln\left(\frac{n_f}{n_i}\right) - \left(1 - \frac{n_{t0}}{n_i}\right)\frac{1}{\alpha}\left[1 - \left(\frac{n_f}{n_i}\right)^\alpha\right] = 0 \tag{2.14}$$

In order to calculate easily measurable laser performance parameters, we create equations that represent laser output energy (E), peak power (P), and approximate pulse duration (W). This is accomplished by the method proposed by Degnan ([8]).

First, the instantaneous laser output power is given by:

$$P(t) = -h\nu Al' \left.\frac{d\phi}{dt}\right|_R \tag{2.15}$$

From Equation 2.1:

$$\left.\frac{d\phi}{dt}\right|_R = -\frac{\phi}{t_r}\ln\left(\frac{1}{R}\right) \tag{2.16}$$

so that for this rate equation model, the instantaneous laser output power is:

$$P(t) = \frac{h\nu Al}{\gamma t_r}\ln\left(\frac{1}{R}\right)\left[n_i - n - n_{t0}\ln\frac{n_i}{n} - [n_i - n_{t0}]\frac{1}{\alpha}\left(1 - \frac{n^\alpha}{n_i^\alpha}\right)\right] \tag{2.17}$$

The peak power is then $P(t)$ when the population inversion is n_t [11]:

$$P = \frac{h\nu Al}{\gamma t_r}\ln\left(\frac{1}{R}\right)\left[n_i - n_t - n_{t0}\ln\frac{n_i}{n_t} - (n_i - n_{t0})\frac{1}{\alpha}\left(1 - \frac{n_t^\alpha}{n_i^\alpha}\right)\right] \tag{2.18}$$

The expression for laser pulse energy (E) is obtained by integrating the instantaneous power from $t = 0$ to $t = \infty$:

$$E = \int_0^\infty P(t)dt = \frac{h\nu Al'\ln\left(\frac{1}{R}\right)}{t_r}\int_0^\infty \phi(t)dt \tag{2.19}$$

Using Equation 2.2 to change the variable of integration, Equation 2.19 becomes [11]:

$$E = \frac{h\nu Al'\ln\left(\frac{1}{R}\right)}{\gamma\sigma ct_r}\int_{n_f}^{n_i}\frac{dn}{n} = \frac{h\nu A}{2\sigma\gamma}\ln\left(\frac{1}{R}\right)\ln\left(\frac{n_i}{n_f}\right) \tag{2.20}$$

From this expression, we can obtain laser fluence (F), an area normalized expression of the laser energy:

$$F = \frac{h\nu}{2\sigma\gamma} \ln\left(\frac{1}{R}\right) \ln\left(\frac{n_i}{n_f}\right) \tag{2.21}$$

Laser pulse duration (W) is approximated using the previous derived quantities, energy (E) and peak power (P). If we assume the pulse width is approximated by a triangle with a height of P, base width t_p, and area E, then the full duration half-maximum (FDHM) of the laser pulse is:

$$W \approx \frac{t_p}{2} = \frac{E}{P} \tag{2.22}$$

We could increase the accuracy of this pulse duration calculation by assuming a Gaussian pulse shape and using the peak power and pulse energy to calculate the pulse duration. In fact, using a Gaussian pulse shape would reduce the pulse duration calculation by about 6%. However, we use the estimate of Equation 2.22 to preserve the simplified rate equation model presentation of [11].

Each of the equations for energy, power, and pulse duration describe an easily measurable and important property of a pulsed laser. It is these expressions that are used to quantitatively describe the performance of the lasers studied in this thesis. The following chapters discuss the methods for experimental measurement of these parameters for Cr^{4+}:YAG Q-switched Cr:Nd:GSGG lasers as well as the resulting agreement of the measurements with the corresponding rate equation calculations.

2.2   General Results of the Rate Equation Model

The ability to analyze the effect that various parameters have on laser output is of great use when designing lasers for specific applications. Using the rate equations,

it is possible to develop an understanding of the expected performance as well as operating requirements of various laser designs.

The equations that result from analytically solving the rate equation model provide a means to study the behavior of Q-switched lasers across various design parameters. The two central design parameters, T_0 and R_{OC}, are of particular interest because they have an interrelated and non-linear affect on the output of Q-switched lasers and are the basic design parameters studied in this thesis. Understanding the effect that these parameters have on laser performance provides a valuable design tool for Q-switched lasers.

The figures in this section were prepared with the aid of computer routines used to solve the transendental equations presented in Section 2.1. These curve sets were produced by calculating solutions to the rate equations for a range of T_0 and R_{OC} and using the material parameters associated to a Cr:Nd:GSGG laser Q-switched by Cr^{4+}:YAG. Table 2.2 shows the input parameters to the rate equation model as used in this thesis, using other laser or Q-switch material values will yield different design curves.

Gain medium length	6 mm
Air gap between laser and Q-switch	2 mm
Laser rod active diameter	0.27 mm
Wavelength	1061 nm
Double pass resonator loss	5%
Laser stimulated emission cross section	1.57e-19 cm^2
Inversion reduction factor (γ)	1
Speed of light (c)	3e10 cm·s^{-1}
Cr:Nd:GSGG index of refraction	1.942
Cr^{4+}:YAG index of refraction	1.82
Q-switch ground state absorption cross section (σ_{13})	8.7e-19 cm^2
Q-switch excited state absorption cross section (σ_{24})	2.2e-19 cm^2
Q-switch total population density (n_{s0})	2.15e18 cm^{-3}

Table 2.2: Input parameter values used in the rate equation model calculations.

As an example of the rate equation model output, Figures 2.1 and 2.2 illustrate the laser Q-switched calculated energy fluence and pulse duration as a function of the Q-switch T_0 and resonator R_{OC} over a range inclusive of the experimental lasers examined herein (See Chapter 3). These curves are made by using the material parameters of Table 2.2 to produce values for the transcendental Equations 2.13 and 2.14. Plugging these values into Equations 2.18, 2.20, and 2.22, for a large range of T_0 and R_{OC}, provides the data presented in Figures 2.1 and 2.2.

The curves show that there is significant difference in the calculated performance of a passively Q-switched laser, even for small variations in the design parameters. A change in the output mirror reflectivity of 30% can easily double the laser energy. The rate equation model estimates also show that the pulse duration of a passively Q-switched laser increases exponentially with Q-switch initial transmission and is linearly dependent on output coupler reflectivity.

Estimates can also be created from the rate equation model for important laser output and operational characteristics, such as laser efficiency and pump power requirements. This is done by first calculating the stored energy in the laser as the initial population inversion density times the gain volume times the energy of a photon. Extending the stored energy calculation, estimates can be produced of several parameters, including laser extraction efficiency (Figure 2.3), by calculating the ratio of the stored energy to the Q-switched energy, and the pump power requirements (Figure 2.4), by calculating the necessary pump power to produce the estimated stored energy. Use of the rate equation model for these calculations ignores some of the energy lost in non-radiative processes and to spontaneous emission in the gain material, but serves as an estimate for laser system design.
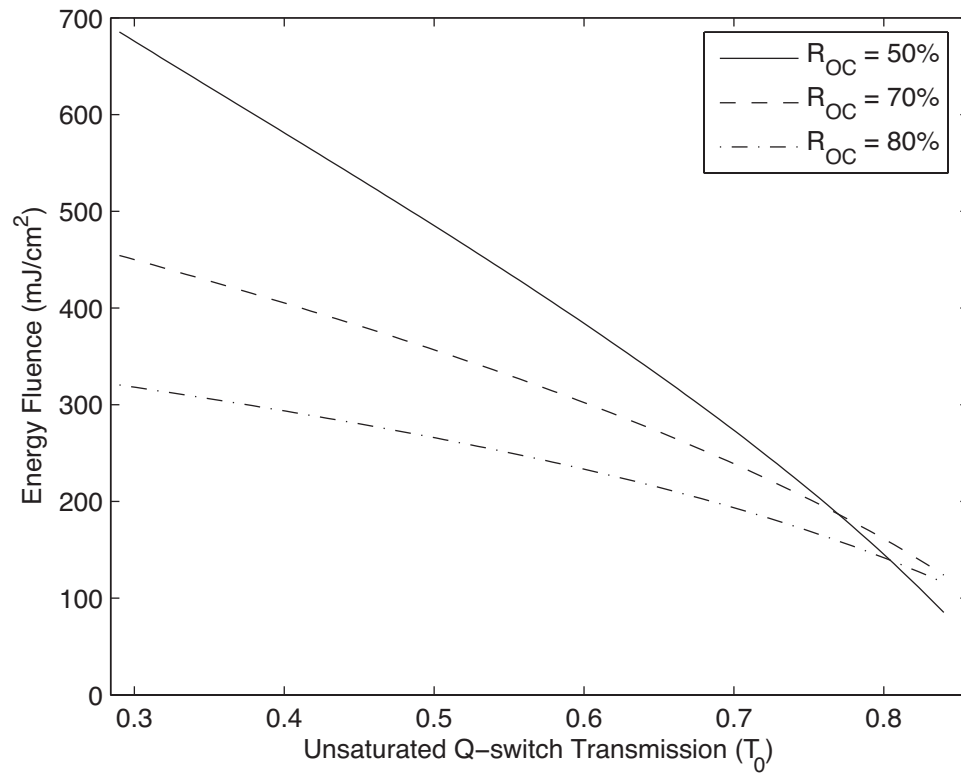
Figure 2.1: Cr:Nd:GSGG, Cr^{4+}:YAG Q-switched laser rate equation model calculated energy fluence plotted against the saturable absorber initial transmission and resonator output coupling.
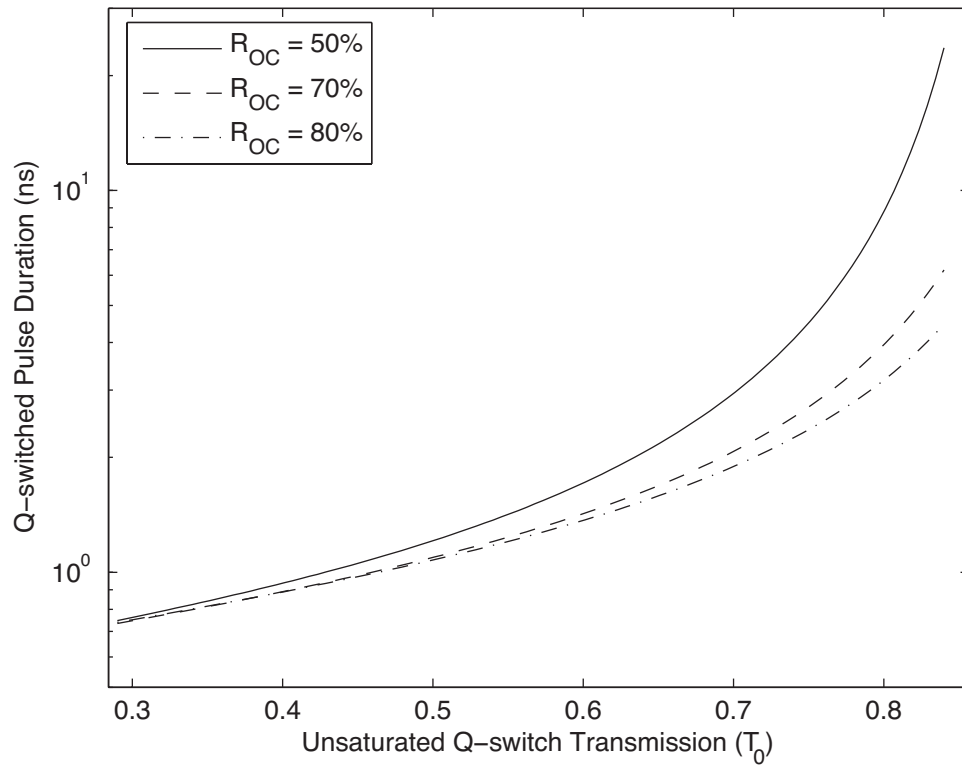
Figure 2.2: Cr:Nd:GSGG, Cr^{4+}:YAG Q-switched laser rate equation model pulse duration plotted against the saturable absorber initial transmission and resonator output coupling.

Figure 2.3: Rate equation model extraction efficiency for Cr:Nd:GSGG, Cr^{4+}:YAG Q-switched laser plotted against the saturable absorber initial transmission and resonator output coupling.

Figure 2.4: Rate equation model estimated pump power needed for Cr:Nd:GSGG, Cr^{4+}:YAG Q-switched laser operation plotted against the saturable absorber initial transmission and resonator output coupling.
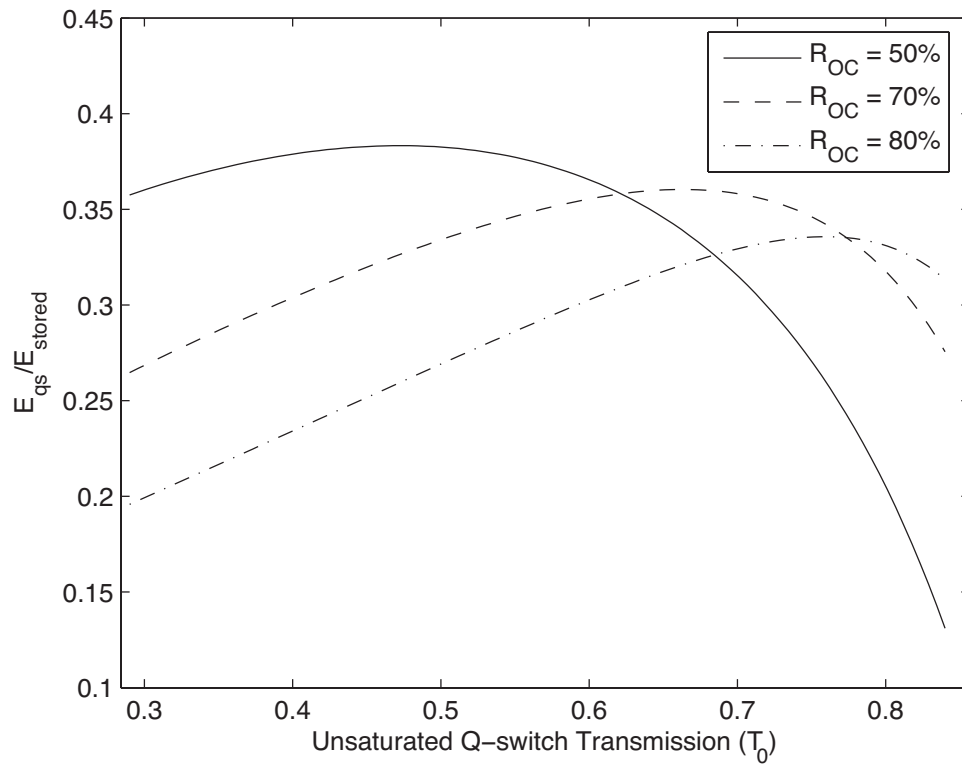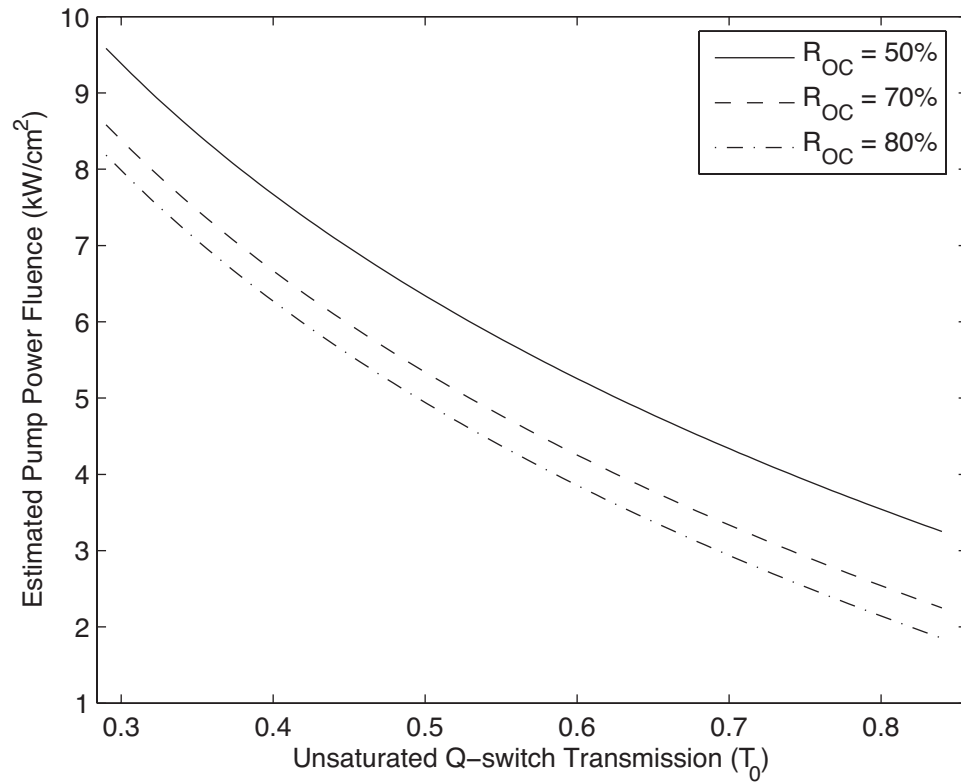
Chapter 3

Experimental Hardware and Data Collection

3.1 Microlasers

In order to assess the ability of the rate equation model to calculate performance of passively Q-switched microlasers, we experimentally studied nine lasers with unique combinations of Q-switch initial transmission (T_0) and laser cavity output reflectivity (R_{OC}). These values, shown in Figure 3.1, allow us to analyze the model's performance in a large portion of the laser design space.

The nine lasers are composed of two crystals (the laser and Q-switch materials) and two resonator mirrors that are coated directly onto the crystal faces. The laser rod material is Cr:Nd:GSGG, and the Q-switch is Cr^{4+}:YAG. The input mirror to the resonator has high reflectivity (HR) coating at the laser wavelength, 1061 nm, and an anti-reflectivity (AR) coating at the pump wavelength, 808 nm. The resonator output mirrors have various partial reflectivity output coupler coatings at 1061 nm (see Figure 3.1). The mirror coatings are applied directly to the flat laser and Q-

Laser #	R_{OC}	T_0
1	50%±3%	30%±3%
2	50%±3%	50%±3%
3	50%±3%	65%±3%
4	50%±3%	80%±3%
5	80%±3%	30%±3%
6	80%±3%	50%±3%
7	80%±3%	65%±3%
8	80%±3%	80%±3%
9	70%±3%	65%±3%

Table 3.1: Initial transmission and output coupler reflectivity of the nine laser systems studied. The lasers shown in gray are subject to high intracavity fluence levels and did not produce data. This is discussed further in Section 3.4.

switch crystal surfaces, create a flat-flat laser cavity.

Lasers one through eight were created using an interchangeable Q-switch laser system. This system, shown in Figure 3.1, provides eight different lasers, with unique T_0 and R_{OC} combinations, using a single laser rod, 2.5 mm in diameter and 6.0 mm in length, and eight interchangeable Q-switch crystals, 4.0 mm in diameter with a length inversely proportion to the T_0 of the Q-switch. Each Q-switch crystal has one of four T_0 values and a mirror coated to the output face with one of the two R_{OC} values as described in Table 3.1. The cavity alignment is accomplished through a mounting bracket designed to allow 2-axis movement of the Q-switch relative to the laser rod.

The ninth laser system is composed of Cr:Nd:GSGG and Cr^{4+}:YAG diffusion bonded together with a section of undoped YAG on the input side of the laser rod. The additional crystal acts as a heat sink, improving heat diffusion from the pump face of the laser material, when the laser system is operated at a high rep rate. The additional undoped YAG crystal does not affect the operation of the laser system at the low rep rates which allow thermal energy to dissipate between shots. For this
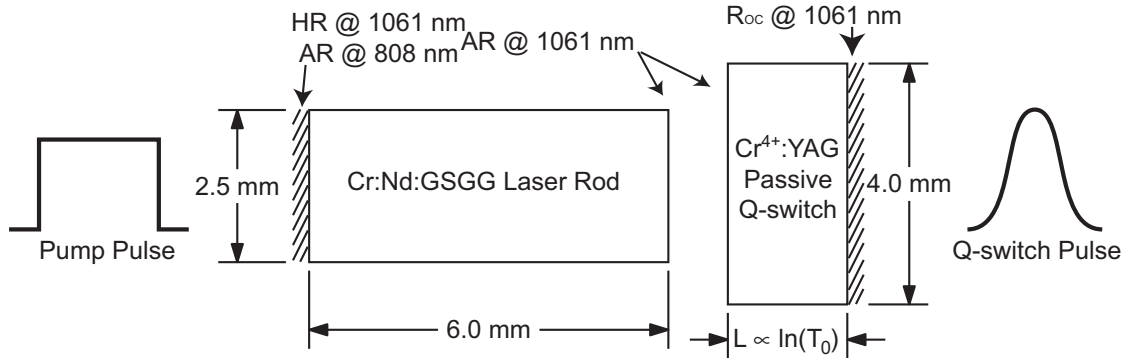
Figure 3.1: Schematic of the interchangeable laser rod/Q-switch system. Eight Q-switch crystals, each with one of four T_0 values and one of two R_{OC} values coated onto the crystal face, provide multiple lasers with unique T_0 and R_{OC} values to be studied.

reason, laser operation is held to 10 Hz for the observations in this thesis. A schematic of this monolithic laser system is shown in Figure 3.2. The 5.0 mm diameter bonded crystal is a total of 9.5 mm long. It is made up of 1.0 mm of undoped YAG, 7.0 mm of Cr:Nd:GSGG laser material, and 1.5 mm of Cr^{4+}:YAG passive Q-switch providing T_0 of 65%. Alignment of these diffusion bonded crystals is provided by the tolerances of the manufacturing process.
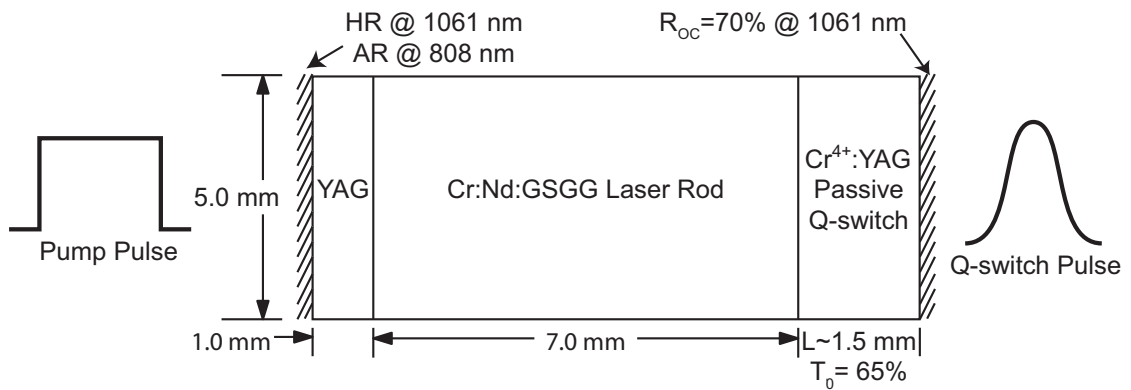

Figure 3.2: Schematic of the monolithic laser system. Laser number nine is composed of diffusion bonded undoped YAG (to aid with heat dissipation in high duty cycle laser systems), Cr:Nd:GSGG laser material, and a Cr^{4+}:YAG Q-switch.

3.2   Laser Pumping

The lasers investigated in this thesis are laser diode end-pumped systems. To ensure laser operation in the TEM_{00} mode, only a small cross section of the laser input face is pumped. With the relatively low energy requirements of a small diameter end-pumped system, a temperature-controlled 60 W fiber-coupled laser diode was chosen as the pump source.

The pump system, shown in Figure 3.3, employs a short focal length lens to couple the output energy of the laser diode into the microlaser. The spacing of the output fiber, lens, and microlaser are experimentally determined to maximize the energy deposited in the TEM_{00} mode of the microlaser, with representative dimensions illustrated in Figure 3.3

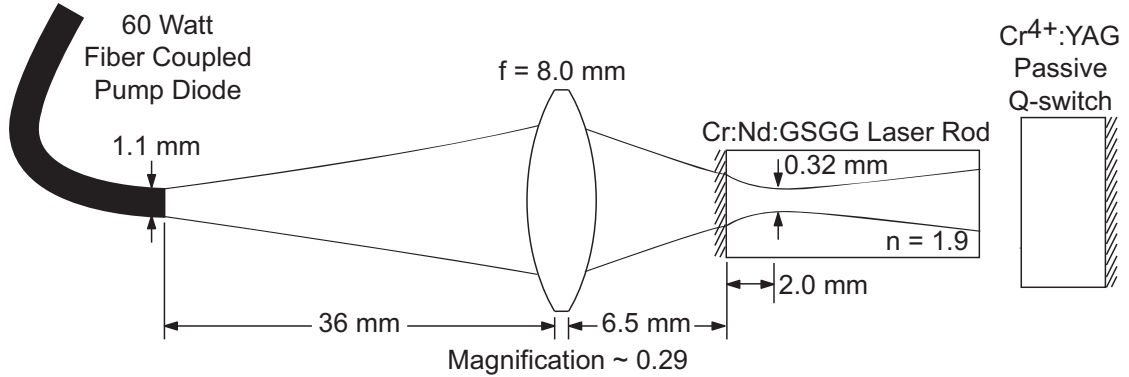Figure 3.3: Lens coupling of laser diode energy into the microlaser resonator. The end pumped laser diode energy is deposited such that the gain volume overlaps the fundamental laser mode to produce TEM_{00} laser output.

3.3   Laser Characterization

Measurements of the pulse fluence and duration are collected from the studied lasers. A figure of the laboratory setup used for data collection is provided in Figure 3.4.

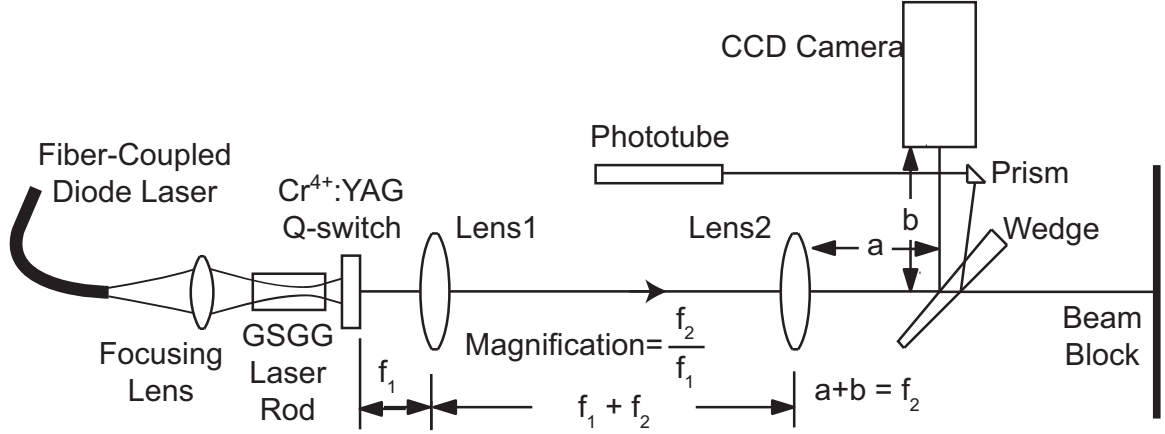The collected data is presented in Section 4.1.

Figure 3.4: Schematic of the system used to characterize the microlasers. Laser fluence was calculated from separate beam energy and diameter measurements. The relay imaging system (magnification is equal to the focal length of lens two (f_2) divided the focal length of lens one (f_1): magnification=f_2/f_1) allowed the CCD camera to maximize available resolution when imaging the laser output coupler.

Pulse fluence, the area normalized laser energy, is calculated from two separate laboratory observations: laser pulse energy and diameter. The diameter measurement allows us to calculate a beam area. Dividing this into the beam energy, the pulse fluence is calculated. The fluence measurement error is calculated by propagating the error associated with the composite measurements through the fluence calculation (fluence=energy/area). Equation 3.1 is the error propagated calculation for the fluence error (ΔF), where F, E, and D are the absolute measurements of the fluence, energy, and diameter of the laser pulse. Δ denotes the error value of each measurement. The measured and calculated values for all measurements are reported in Section 4.1. The energy and diameter measurements are described below.

$$\Delta F = F\sqrt{\left(\frac{\Delta E}{E}\right)^2 + \left(\frac{2\Delta D}{D}\right)^2} \qquad (3.1)$$

The pulse energy is measured by utilizing independently calibrated pyroelectric

and photodiode detectors. Stray energy from the pump system is prevented from entering the measurement detectors by utilizing a blocking filter at the pump wavelength. Pulse measurements presented are an average of 100 laser pulses. The laser pulse energy is extremely stable shot-to-shot, with a standard deviation of 1 μJ. Therefore, the energy measurement error is dominated by the calibration error ($\pm 3\%$) of the detectors.

Beam area is determined by measuring the $1/e^2$ beam diameter with a CCD camera and BeamView laser profiling software from Coherent. Using a simple two lens relay imaging system to project a magnified image (magnification is equal to the focal length of lens two (f_2) divided the focal length of lens one (f_1): magnification=f_2/f_1) of the laser beam onto the CCD camera, and thereby maximize utilization of available CCD resolution, the camera records the two-dimensional intensity profile of 100 laser pulses at the output coupler. Computer routines are then used to fit a Gaussian profile to the beam cross sections. The aggregate $1/e^2$ width and standard deviation of the Q-switch pulses is then calculated. The laser beam has a half-angle divergence of approximately 2.5 mR. Coupled with relay imaging optics of 1" in diameter and component lenses with focal lengths of less than 500 mm, there is negligible energy lost to the imaging system.

Verification of the CCD beam diameter measurement included both direct measurement of the laser beam at the output coupler and independent verification of the relay imaging system. The beam diameter was directly measured by scanning a razor blade across the face of the output coupler. This measurement was performed by masking an incrementally larger area of the laser beam cross section and measuring the transmitted intensity. The beam diameter is then calculated from the resulting intensity profile. We also imaged a standard commercial resolution target through the magnified relay imaging system used to measure the laser output. The measured diameter of both methods matched the magnification corrected measurement of the

CCD camera.

Pulse duration is measured as the full duration half-maximum (FDHM) of the laser output pulse. Each reported measurement is made on an oscilloscope pulse trace that is the average of 100 individual laser pulses. The pulse duration data is collected through a 60ps rise time phototube connected to an oscilloscope with a maximum sample rate of 5 GSa/s and an interpolated resolution determined by the time scale. The oscilloscope resolution is then combined with the random error, which is observed to be less than 1% of the measured duration, to calculate the reported pulse duration error. The pulse duration measurement methodology is discussed further in Appendix A.

3.4 Data Limitations

A total of nine lasers were studied. However, due to issues with the preexisting laser systems used in this thesis, data could not be taken from five of these lasers. The intracavity fluences produced by lasers 1, 2, 5, 6, and 7 caused damage to the crystal coating. When the estimated damage threshold of 0.66 GW/cm^2 was exceded by a laser's intracavity fluence, it caused ablation of the crystal surface coatings and prevented laser operation. The resonators that were affected are shown with a gray background in Table 3.1.

Figure 3.5 shows the peak intracavity power fluence of a passively Q-switch Cr:Nd:GSGG, Cr^{4+}:YAG laser as a function of T_0 and R_{OC}. The curves and data points are calculated using the rate equation model described earlier. Equation 2.18 describes the peak power coupled from the microlaser cavity. Defining P_{output} as the area scaled peak power of 2.18, the peak power fluence inside the laser resonator is:

$$P_{intracavity} = \frac{P_{output}}{1 - R_{OC}} \tag{3.2}$$

where $P_{intracavity}$ is the peak intracavity power fluence, P_{output} is the peak power fluence coupled from the cavity, and R_{OC} is the microlaser output coupler reflectivity.
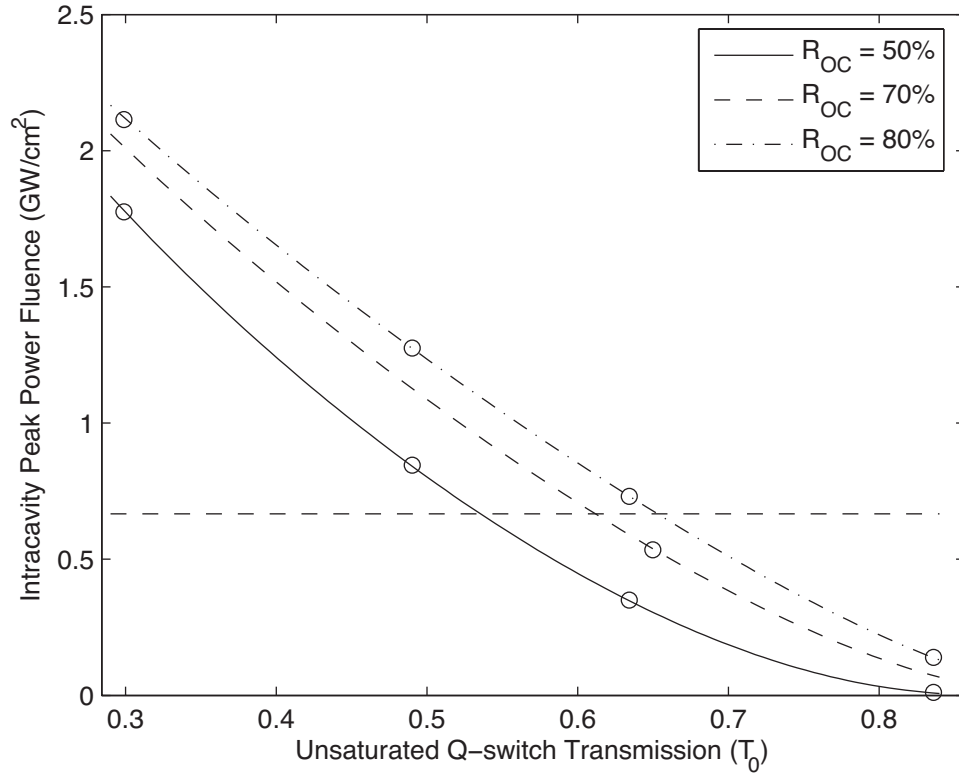
Figure 3.5: Calculated intracavity peak power fluence as a function of the Q-switch initial transmission (T_0) for three different values of output coupling (R_{OC}). The data points represent the calculated intracavity peak power fluence for the laser configurations studied. The horizontal line corresponds to the calculated damage threshold of the laser cavity coatings.

The damage fluence threshold for the studied laser resonator coatings is specified as 10 J/cm^2 with a pulse length of 10-15 ns. These numbers correspond to a damage threshold power between 0.66 GW/cm^2 and 1 GW/cm^2. The lower estimated damage threshold of the laser resonator coatings is represented in Figure 3.2 by the horizontal line.

The calculated intracavity peak power fluence of the nine laser configurations

available is represented in Figure 3.5 by circle makers. Comparing the calculated peak power fluence values with the damage threshold of the crystal coatings, we see that the rate equation model predicts five of the nine available lasers will produce higher intracavity power densities than the resonator coating are designed to withstand. This agrees with our laboratory observations. All laser configurations which lie above the horizontal line of Figure 3.5 caused damage to the laser crystal coatings. This coating ablation caused these lasers to be inoperable, leaving four operating lasers that produced data.

Chapter 4

Data Results and Conclusions

4.1   Data Reduction

Due to the complicating issues mentioned in the previous section, model performance is evaluated using information from four lasers. These lasers are the three interchangeable laser configurations with the lowest intracavity power density as well as the monolithic laser described earlier.

From the four lasers able to produce data, nine experimental data sets are presented. After the first data sets were collected from lasers three, four, and nine, we collected additional data sets from all lasers, which resulted in duplicate measurements for three lasers. These duplicate measurements are not averaged because there are variations in the pump system used between measurements. These variations induce differences in the diameter of the transverse laser mode. The additional data sets serve as both verification of measurement methodologies and corroboration of the model fit evaluation for small variations in the pump laser and coupling optics. The implication of these variations will be discussed further in Section 4.4.

Table 4.1 presents the four measured values of pulse energy, diameter, fluence, and duration from the four evaluated lasers. In addition, difference (Δ) and percent deviation values are calculated from the rate equation model (REM) calculations of fluence and pulse duration. The term percent deviation describes the variation of the measured laser data from the rate equation model calculations as shown in Equation 4.1. It describes the variation of the measured data from a baseline value that is provided by the rate equation model.

$$\% \text{ deviation} = \frac{(measured\ data\ value) - (REM\ value)}{(REM\ value)} \cdot 100\% \tag{4.1}$$

To aid in the data analysis, three data plots are provided. Figures 4.1 and 4.2 plot the correlation of the laser pulse fluence and duration data to the rate equation model calculations. The two plots show the rate equation model calculations on the horizontal axis and the corresponding measured data on the vertical axis for each of the seven data sets. This yields a figure in which a perfect correlation between the observed data and the calculated values would yield a line of data points from the origin with a slope of one. In addition, the pulse duration data is presented in Figure 2.2 plotted against the rate equation model calculation curves for the Q-switched laser pulse duration as a function of the two major laser design parameters, R_{OC} and T_0.

From the presented data, we discuss three observations. These discussions are of the rate equation model correlation to the measured fluence data and measured pulse duration data as well as and the effect that transverse laser mode diameter has on these observations.

Data Set #	1	2	3	4
Laser #	3	3	4	4
Q-switch T_0	63.4%	63.4%	83.6%	83.6%
Q-switch R_{OC}	51.8%	51.8%	51.8%	51.8%
Pulse Energy (μJ)	162±5	177±5	50±2	47±1
Beam Diameter (mm)	0.26±0.04	0.25±0.04	0.30±0.04	0.27±0.04
Pulse Fluence (mJ/cm^2)	305±94	361±116	71±19	82±24
Pulse Duration (ns)	1.0±0.1	1.2±0.1	1.8±0.1	2.0±0.2
REM Fluence (mJ/cm^2)	345	345	98	98
REM Pulse Duration (ns)	2.0	2.0	17.3	17.3
Fluence Δ (mJ/cm^2)	-40	16	-27	-16
Fluence % deviation	-12%	4.5%	-28%	-16%
Pulse Duration Δ (ns)	-1.0	-0.8	-15.5	-15.3
Pulse Duration % deviation	-50%	-40%	-90%	-88%
Data Set #	5	6	7	
Laser #	8	9	9	
Q-switch T_0	83.0%	65.0%	65.0%	
Q-switch R_{OC}	81.8%	70.0%	70.0%	
Pulse Energy (μJ)	55±2	97±3	877±26	
Beam Diameter (mm)	0.29±0.01	0.24±0.01	0.62±0.06	
Pulse Fluence (mJ/cm^2)	83±6	214±19	290±57	
Pulse Duration (ns)	3.4±0.1	0.8±0.3	1.2±0.1	
REM Fluence (mJ/cm^2)	119	272	272	
REM Pulse Duration (ns)	3.9	1.7	1.7	
Fluence Δ (mJ/cm^2)	-36	-58	18	
Fluence % deviation	-30%	-21%	6.8%	
Pulse Duration Δ (ns)	-0.5	-0.9	-0.5	
Pulse Duration % deviation	-13%	-54%	-31%	

Table 4.1: Fluence and pulse duration data for the seven collected data sets, the corresponding rate equation model (REM) calculations, and calculations of the correlation parameters % deviation and difference (Δ).

4.2   Laser Fluence Data

The data plotted in Figure 4.1 shows that there is a reasonable correlation of the measured data to the ideal fit line. With a maximum deviation from the rate equation model calculation of 30%, the measured fluence data generally fits well with the

model. The plotted data points generally overlay the ideal fit line well with no evidence of a systematic error across the data sets.
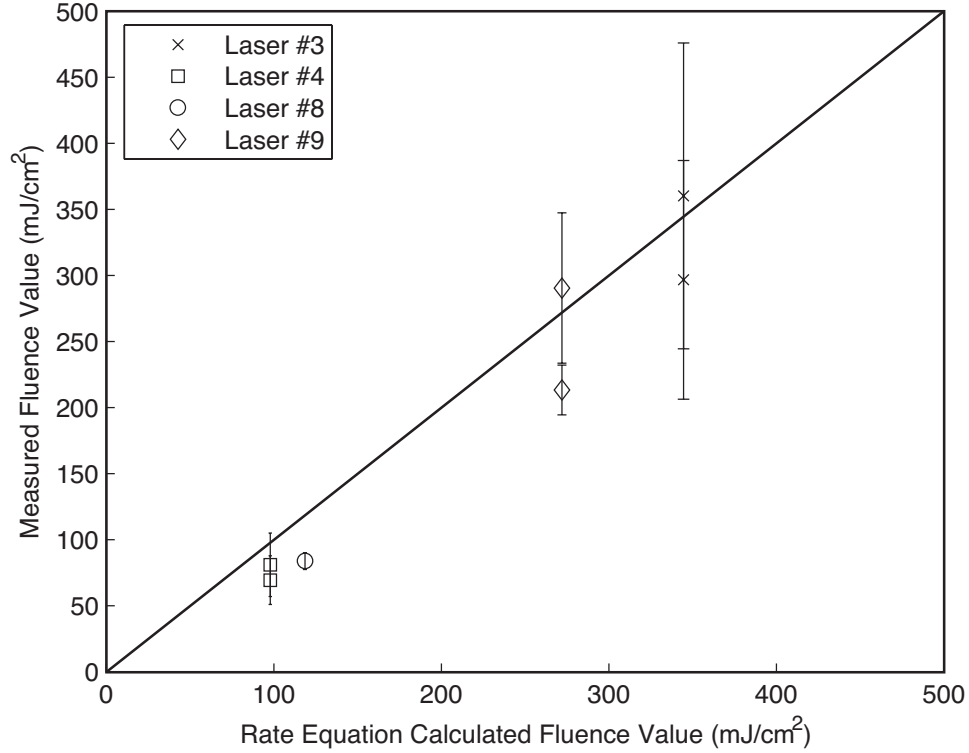

Figure 4.1: Rate equation model calculated pulse fluence plotted against the measured fluence data sets. An ideal fit would place the plotted data points on the linear line denoting equal measured and calculated pulse fluence values. The plotted data overlays well with the ideal fit line and show no systematic error.

One item of particular interest is the increase in measurement error that exists with higher fluence values. This increase is driven by the ±3% measurement error of the energy meters used in the data collection. This propagates through the fluence calculations and, combined with the inaccuracy in the diameter measurement, produces increasing fluence error values that scale with the fluence magnitude. Despite this increase in measurement uncertainty at higher fluence values, the data is evenly distributed on each side of the ideal fit line and no systematic errors are evident.

4.3   Pulse Duration Data

The rate equation model consistently overcalculates pulse duration values for all data sets. As can be seen in Figure 4.2, all the pulse duration data is well below the ideal fit line. Higher deviation from the rate equation model is expected for the measured pulse duration data than is expected for the fluence measurements because the pulse duration calculation is fundamentally an estimation (as described in Chapter 2). However, there is a significant negative systematic error across all pulse duration data that can not be accounted for by this estimation.
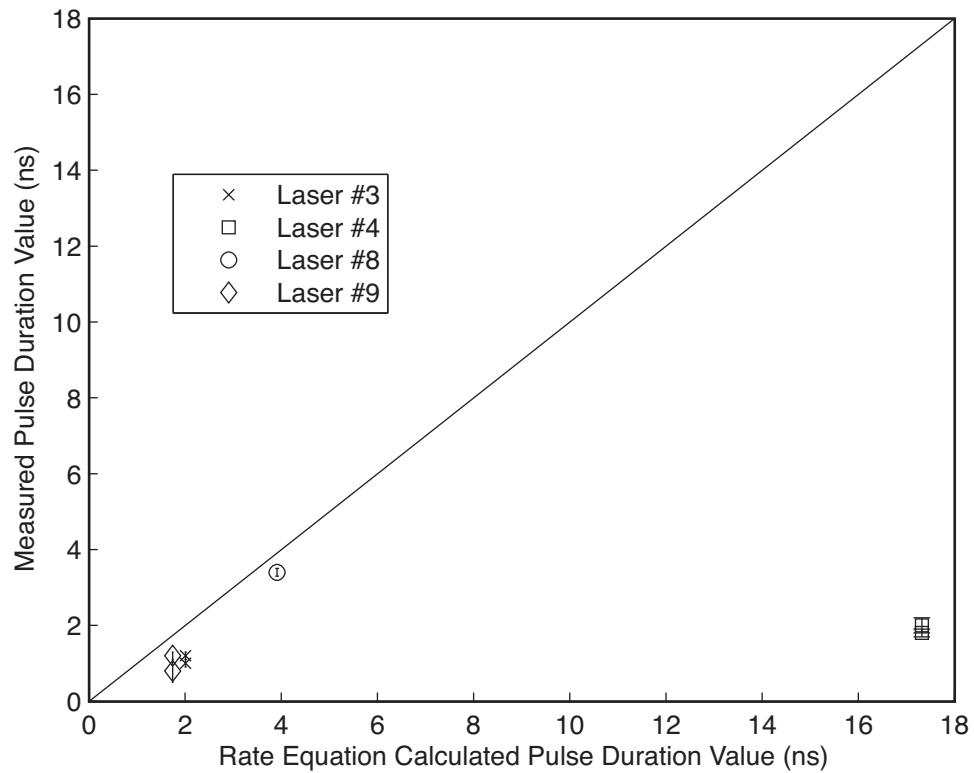

Figure 4.2: Rate equation model calculated pulse duration plotted against the pulse duration data sets. An ideal fit would place the plotted data points on the linear line denoting equal measured and calculated pulse duration values. The measured data shows significant deviation for Laser #4. Figure 4.3 provides more resolution into this discrepancy.

In addition to the systematic error evident across all data, data sets #3 and #4 show a significantly higher deviation from the rate equation model calculations than the other data sets. In order to better analyze the implications of this deviation, we plot the pulse duration data against the laser resonator output coupling reflectivity (R_{OC}) and Q-switch initial transmission (T_0) in Figure 4.3.
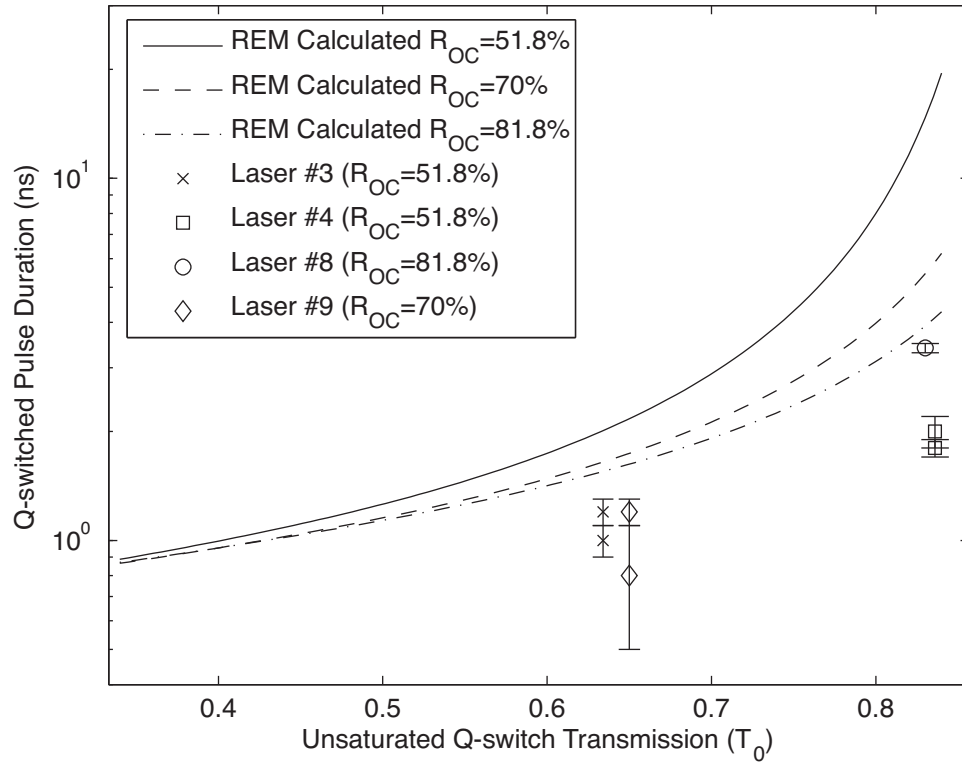

Figure 4.3: Measured pulse duration data overlaid onto rate equation model calculated curves for R_{OC} values of 50%, 70%, and 80%. The plotted data shows significant systematic deviation from the rate equation calculated curves. In addition, measurements for laser #4 do not show the lengthening in pulse duration calculated by the rate equation model.

With the data plotted in this manner, we can see that it does not show the dependence on R_{OC} that the rate equation model calculations predict. The data from lasers with lower R_{OC} values do not show the increasing pulse duration that the rate equation model predicts. This is evident in Figure 4.3 with lasers #3 and #9 as

well as lasers #4 and #8 showing similar pulse durations despite their differing R_{OC} values. The difference is particularly evident between the data sets of laser #4 and laser #8. The laboratory measurements show a pulse duration difference between the two lasers of about 1.5 ns, whereas the rate equation model predicts a difference an order of magnitude larger and in the opposite direction.

We can resolve, to some degree, the disagreement between the measured data and the rate equation calculations by using alternate values for the ground and excited state cross sections of the Q-switch as input to the rate equation model. However, the reality is that it is difficult to confidently apply any particular value for the Q-switch cross sections to the rate equation model. It has been shown that these cross sections can vary from manufacturer to manufacturer as well as within production runs from a single manufacturer [36].

To better understand the variation that can be expected from changes to the Q-switch ground and excited state cross sections, we plot the measured data against the calculated rate equation model curves for a set of four cross section values. Figures 4.4, 4.5, and 4.6 plot calculated fluence while Figures 4.7, 4.8, and 4.9 plot calculated pulse duration with the collected data sets overlaid. The six figures provided plot the rate equation calculations for output coupler reflectivity values of R_{OC}=50%, 70%, and 80% for both the pulse fluence and duration. The four sets of cross section values used to create these plots where chosen because they are representative of the values reported in literature. The cross section values and references are given in Table 4.2.

As was discussed in Section 4.2, the measured fluence values fit well with the calculated values when using the cross section (CS) set #3 (the values used to produce the calculations in this thesis), with only laser #8 deviating from the calculated value by more than the error bar. However, the correlation of the fluence data does not translate to the pulse duration data. In fact, measured data generally either fits the

calculated values of pulse fluence or duration for a given CS set, but not both. This is to say that, as shown in Figures 4.4 through 4.9, no single set of cross section values best fits both the fluence and pulse duration data. However, the measured data does generally fall within the corridor created by the four plotted cross section curves.

In order to produce better resolution on the rate equation model's ability to accurately calculate laser performance, an improved understanding of the cross section values and the causes of these values varying between lasers is desirable. We do see the rate equation model accurately calculating fluence values for CS set #3, but additional leeway should be allowed for pulse duration design with deviation up to an order of magnitude evident between the measured pulse duration data and calculated values based on the multiple cross sections of Table 4.2.

Cross Section (CS) Set #	σ_{13}	σ_{24}	Reference
1	1.8e-18	4.0e-19	[36]
2	1.2e-18	4.0e-19	[36]
3	8.7e-19	2.2e-19	[34]
4	3.2e-18	4.5e-19	[35]

Table 4.2: Cross section values used as input to the rate equation model to produce Figures 4.4 through Figure 4.9. The four sets of cross section values where chosen because they are representative of the values reported in literature.

4.4 Transverse Laser Mode Diameter Data

Data sets #6 and #7 have significantly different beam diameter and energy measurements, despite the fact that they are from the same laser. The two data points were pumped using laser diodes and coupling optics that produced thermal and gain profiles in the laser rod with significantly different diameters. The resulting laser beam diameter measurement of data set #7 is approximately twice as large as that
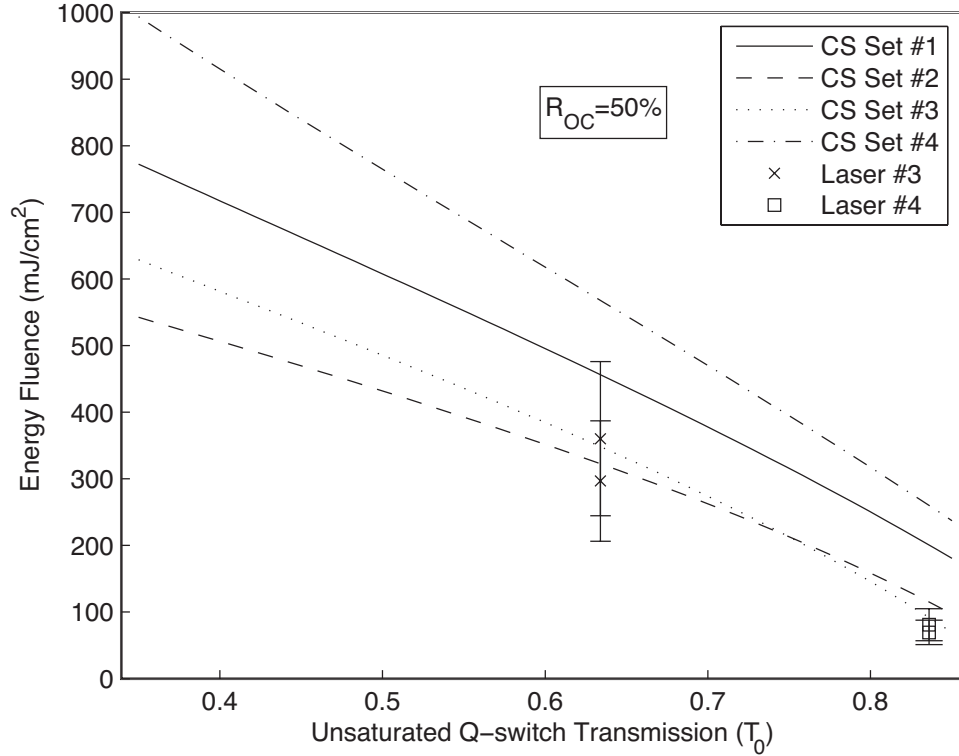
Figure 4.4: R_{OC}=50% rate equation model calculated fluence curves for the four cross section sets given in Table 4.2 with measured data overlaid.

of data set #6. This is due to the thermal resonator effects discussed in Section 1.4.1. Although the beam diameters of the two data sets are significantly different, the resulting fluence is the same. The fact that these two points agree reasonably well with each other, and the rate equation model calculations, is of practical importance providing evidence of rate equation model agreement independent from mode size.

4.5 Conclusions and Future Work

Although the full scope of the planned data sets was not realized, the data gathered shows that the presented plane wave rate equation model provides a reasonable design
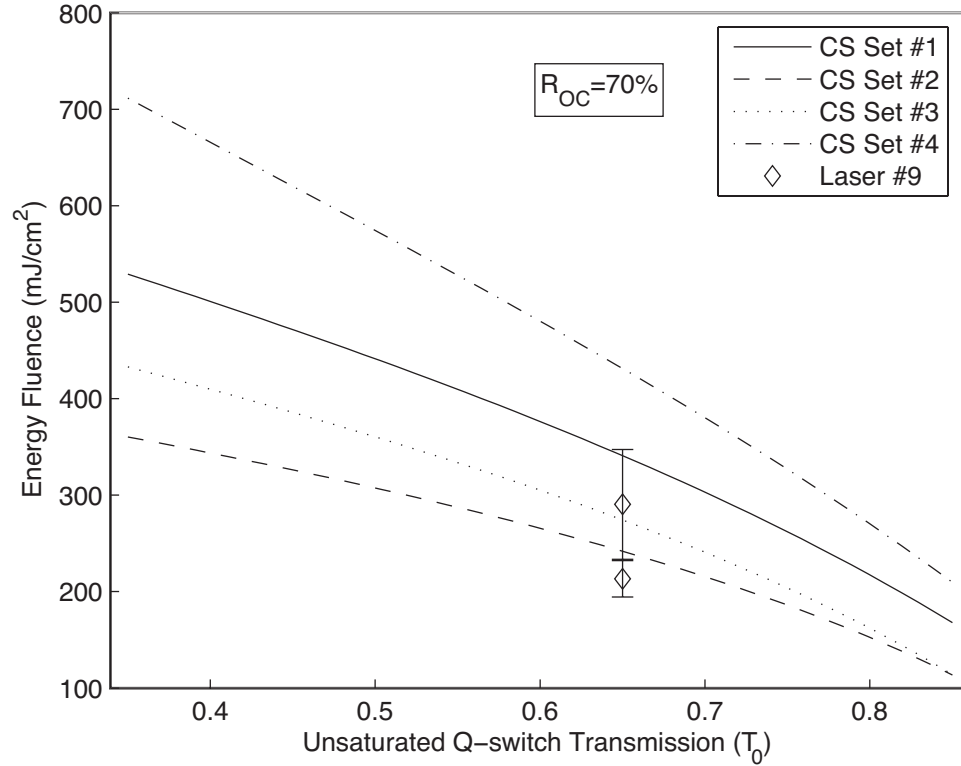
Figure 4.5: R_{OC}=70% rate equation model calculated fluence curves for the four cross section sets given in Table 4.2 with measured data overlaid.

tool for passively Q-switched Cr:Nd:GSGG, Cr^{4+}:YAG lasers. The relatively simple rate equation model allows an engineer to quickly and easily develop calculations of energy, peak power, and pulse duration for a microlaser over a wide range of design parameters, such as T_0 and R_{OC}. The collected data shows that the laboratory fluence measurements deviated from the rate equation model calculations by no more than 30% and that the calculations are independent of mode size for TEM_{00} transverse laser modes. However, the simple rate equation model should not be expected to accurately predict laser pulse duration.

The data presented in this thesis is collected from TEM_{00} Gaussian laser beam profiles. Since the rate equation model used in this thesis is a plane wave model that
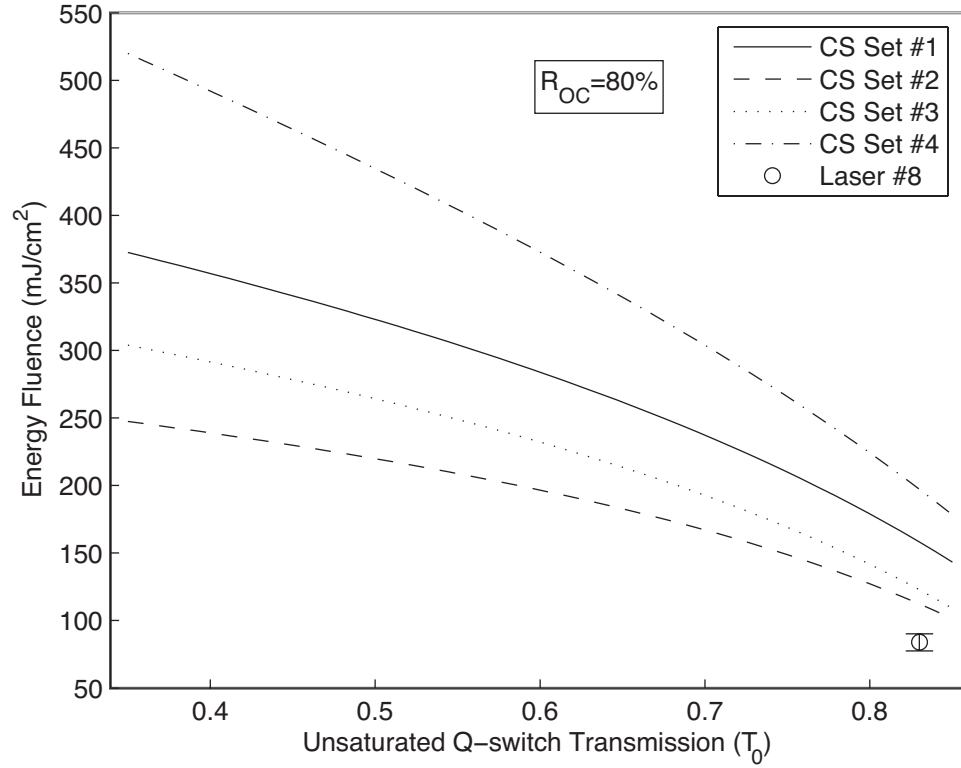
Figure 4.6: R_{OC}=80% rate equation model calculated fluence curves for the four cross section sets given in Table 4.2 with measured data overlaid.

assumes no radial laser intensity variation, it is unclear how well the model calculations hold up when higher order laser modes are present. Although it is possible to preserve TEM_{00} transverse laser modes to some extent by utilizing unstable resonators [44], the study presented in this thesis should be extended to include higher order mode systems in order to confidently apply the simple rate equation model as a design tool to higher energy applications.

Given the inability of the simple rate equation model to accurately calculate pulse duration values, a better understanding of the rate equation model pulse duration calculations should be developed. It is reasonable to look at the Cr^{4+}:YAG Q-switch ground and excited state cross sections, and the variation in published values that
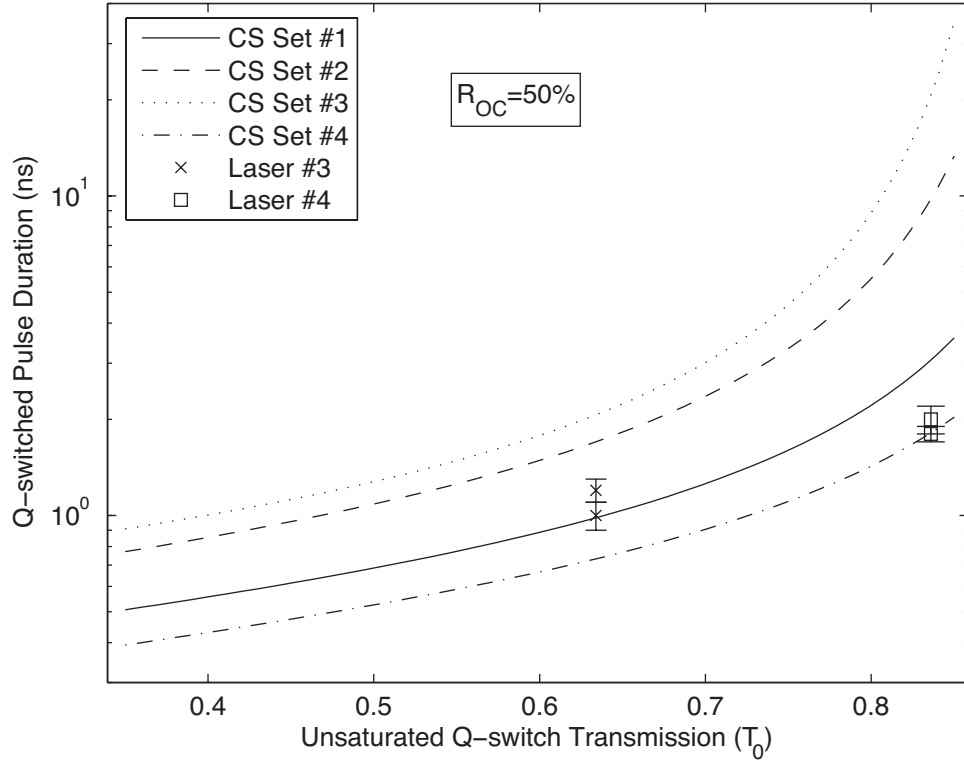
49

Figure 4.7: R_{OC}=50% rate equation model calculated pulse duration curves for the four cross section sets given in Table 4.2 with measured data overlaid.

has been associated to the manufacturing process [36], as a first step to improve this understanding. Given the dependence of the rate equation model on these parameters, a better understanding of their effect on the rate equation calculations and their variation among available materials is necessary to increase confidence in the rate equation model output.
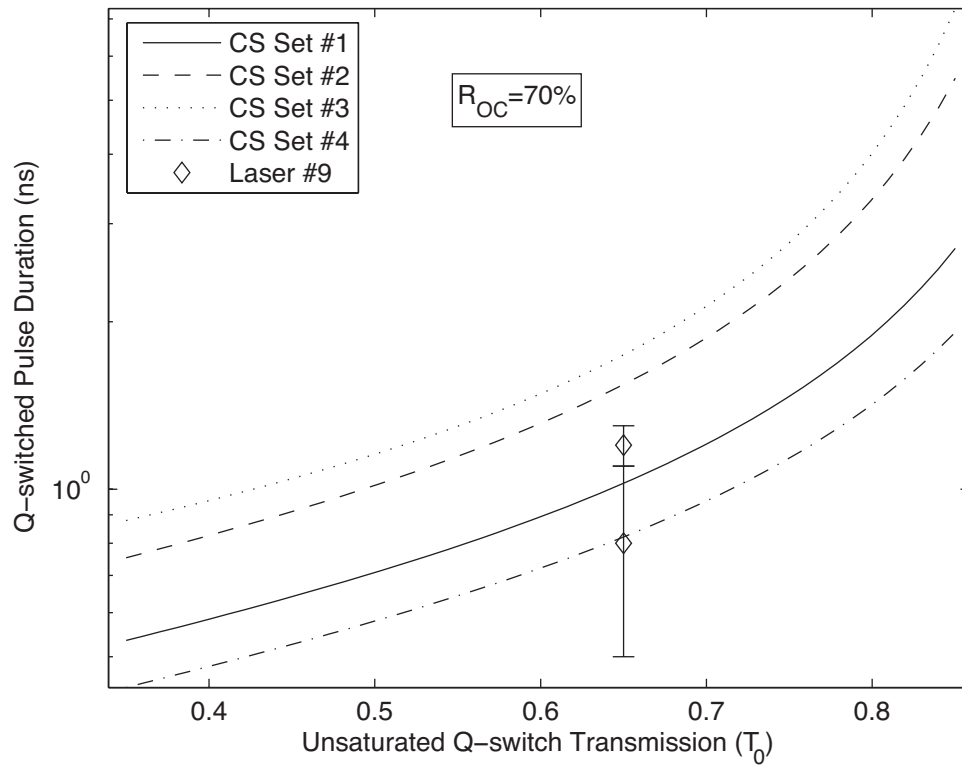
Figure 4.8: R_{OC}=70% rate equation model calculated pulse duration curves for the four cross section sets given in Table 4.2 with measured data overlaid.
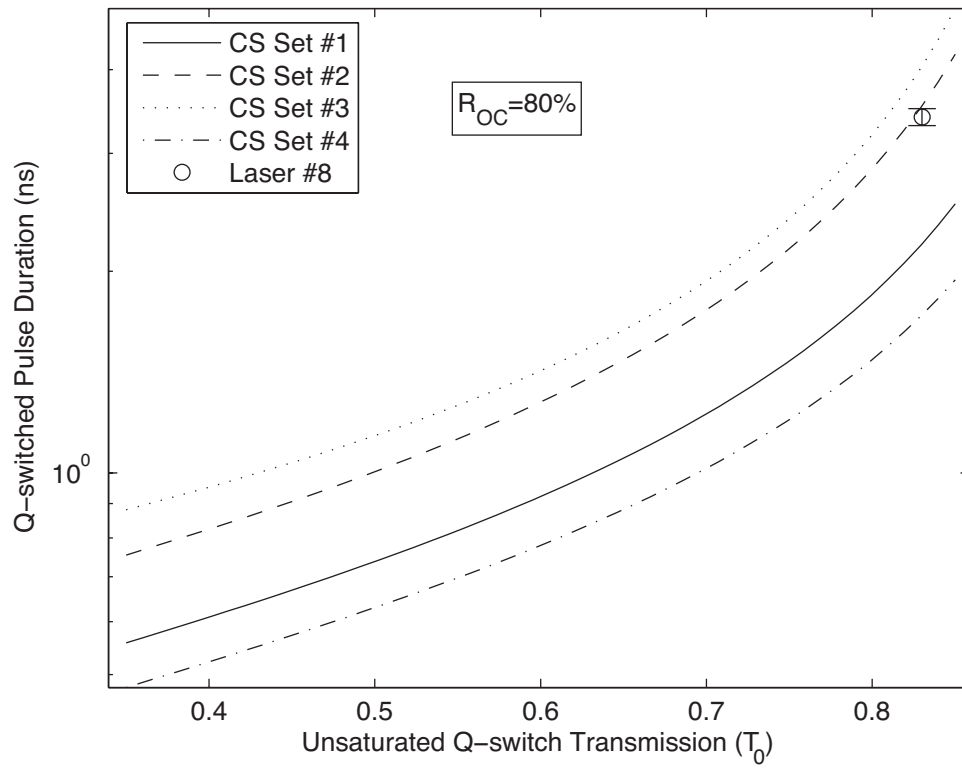
Figure 4.9: R_{OC}=80% rate equation model calculated pulse duration curves for the four cross section sets given in Table 4.2 with measured data overlaid.

Appendices

Appendix A

Verification of Pulse Duration Methodology

In order to ensure the pulse duration measurements of the lasers analyzed in this thesis are not dominated by the response characteristics of the detection system, the impulse response of the pulse duration detection system is measured. The impulse response is determined by measuring the detection system response when excited by a laser independently verified to have a pulse duration of 200 fs.

Figure A.1 shows the impulse response of the pulse duration detection system. The measurement error is based on the bandwidth of the oscilloscope, as described in Section 3.3. The impulse response of the pulse duration measurement system is 0.72±0.02 ns at full duration half maximum. This measurement is based on the interpolated pulse shape of the impulse function on the oscilloscope. This impulse response does not pass the "much less than" criterion for the measured laser duration values that would allow us to neglect the convolution of the detection system's impulse response with the laser pulse.

In order to ensure accuracy of the measured pulse duration data, we estimate the
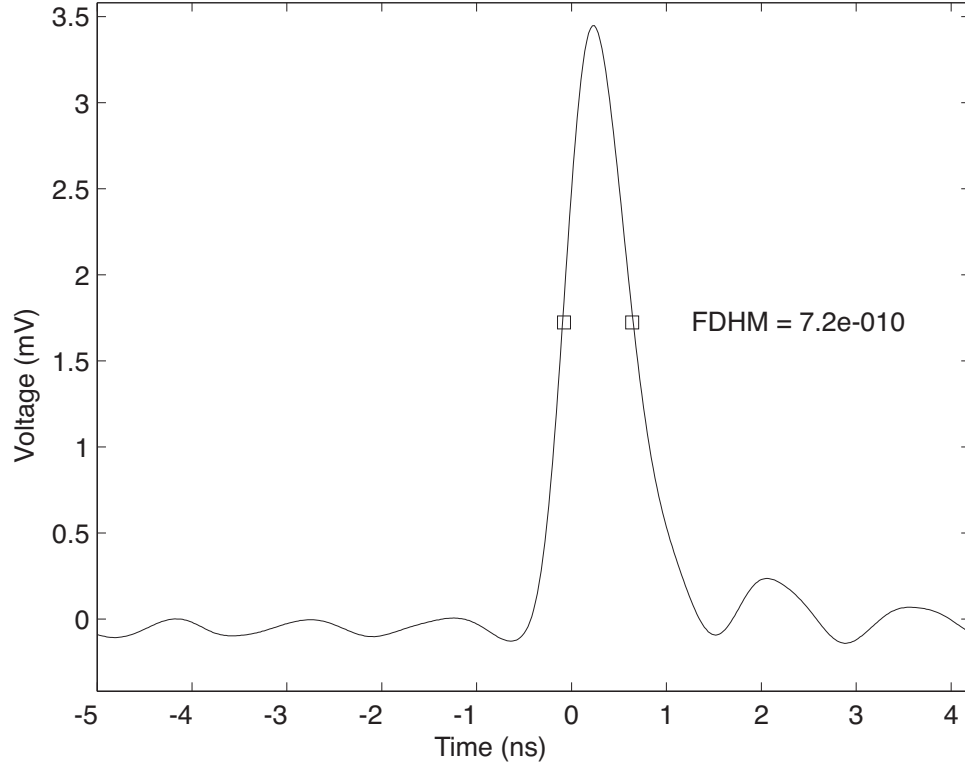
Figure A.1: Impulse response of the pulse duration measurement system. It is determined by measuring the detection system response when excited by a laser independently verified to have a pulse duration of 200 fs.

effect that the detection system's impulse response will have on the measured laser pulses and apply an appropriate correction to the reported data. This is done by deriving the pulse duration relationship of a Gaussian shaped pulse convolved with a Gaussian impulse response.

We assume that the measured data is a convolution of two Gaussian shaped pulses, the input pulse (true laser pulse) and the impulse response of the detection system. Expressed as a function of time (t), a purely Gaussian pulse has the form of Equation A.1, where $\exp{[x]}$ denotes the natural exponential e^x. In this form, P_f is

Appendix A. Verification of Pulse Duration Methodology

the pulse amplitude and τ is the full width at half maximum pulse duration of $f(t)$.

$$f(t) = P_f \exp\left[-4\ln 2\left(\frac{t}{\tau}\right)^2\right] \tag{A.1}$$

Using the convolution of two functions, $f(t)$ and $g(t)$:

$$h(t) = (f \otimes g)(t) = \int_{-\infty}^{\infty} f(t')g(t-t')dt' \tag{A.2}$$

we produce the integral:

$$h(t) = P_f P_g \int_{-\infty}^{\infty} \exp\left[-4\ln 2\left(\frac{t'}{\tau_f}\right)^2\right]\exp\left[-4\ln 2\left(\frac{t-t'}{\tau_g}\right)^2\right]dt' \tag{A.3}$$

From the definite integral:

$$\int_{-\infty}^{\infty} \exp\left[-\left(ax^2 + bx + c\right)\right]dx = \sqrt{\frac{\pi}{a}}\exp\left[\frac{b^2 - 4ac}{4a}\right] \tag{A.4}$$

Equation A.3 becomes:

$$h(t) = P_f P_g \exp\left[-4\ln 2\left(\frac{t}{\sqrt{\tau_g^2 + \tau_f^2}}\right)^2\right] \tag{A.5}$$

From Equation A.5 we see that the pulse duration relationship of two convolved pulses, $f(t)$ and $g(t)$, to the square of the duration of the convolved pulse, $h(t)$, is:

$$\tau_h^2 = \tau_f^2 + \tau_g^2 \tag{A.6}$$

After successfully verifying the results of Equation A.6 with computer based test cases, we applied the results to the measured pulse duration data. The resulting data is reported in Table A.1. Applying the deconvolution of the impulse function from the measured data, based on Gaussian shaped pulses, resulted in an average

Appendix A. Verification of Pulse Duration Methodology

deconvolution compensation of 13% across all seven data sets. As would be expected, the deconvolution compensation for the shorter pulse durations were proportionally larger. The maximum deviation from the measured data is 0.3 ns from data set #6. As shown in the resulting data, there is a non-negligible component of the measured pulse duration data that is a result of the detection system's impulse response. Only the deconvolved pulse duration data from Table A.1 is reported in this thesis.

Data Set #	Laser #	Measured Pulse Duration (ns)	Deconvolved Pulse Duration (ns)
1	3	1.2	1.0
2	3	1.4	1.2
3	4	2.0	1.8
4	4	3.6	3.5
5	8	3.5	3.4
6	9	1.1	0.8
7	9	1.4	1.2

Table A.1: Measured pulse duration data and deconvolved data for the seven data sets reported in this thesis. The deconvolution is based on an impulse response of 0.72 ns as shown in Figure A.1.

References

[1] R. W. Hellwarth. Control of fluorescent pulsations. In *Advances in Quantum Electronics*, pages 344–341. Columbia University Press, 1961.

[2] F. J. McClung and R. W. Hellwarth. Giant optical pulsations from ruby. *Journal of Applied Physics*, 33(3):828–829, March 1962.

[3] R. W. Hellwarth. Theory of the pulsation of fluorescent light from ruby. *Physical Review Letters*, 6:9–12, January 1961.

[4] F.J. McClung and R.W. Hellwarth. Characteristics of giant optical pulsations from ruby. *Proceedings of the IEEE*, 51:46–53, January 1963.

[5] W. G. Wagner and B. A. Lengyel. Evolution of the giant pulse in a laser. *Journal of Applied Physics*, 34(7):2040–2046, July 1963.

[6] R. B. Kay and G. S. Waldman. Complete solutions to the rate equations describing Q-spoiled and PTM laser operation. *Journal of Applied Physics*, 36:1319–1323, April 1965.

[7] A. Szabo and R. A. Stein. Theory of laser giant pulsing by a saturable absorber. *Journal of Applied Physics*, 36:1562–1566, May 1965.

[8] J. J. Degnan. Theory of the optimally coupled Q-switched laser. *IEEE Journal of Quantum Electronics*, 25(2), February 1989.

REFERENCES

[9] J. J. Zayhowski and P. L. Kelley. Optimization of Q-switched lasers. *IEEE Journal of Quantum Electronics*, 27:2220–2225, September 1991.

[10] J. J. Degnan. Optimization of passively Q-switched lasers. *IEEE Journal of Quantum Electronics*, 31:1890–1901, November 1995.

[11] X. Zhang, S. Zhao, Q. Wang, Q. Zhang, L. Sun, and S. Zhang. Optimization of Cr^{4+}-doped saturable-absorber Q-switched lasers. *IEEE Journal of Quantum Electronics*, 33(12):2286–2294, December 1997.

[12] G. Xiao and M. Bass. A generalized model for passively Q-switched lasers including excited state absorption in the saturable absorber. *IEEE Journal of Quantum Electronics*, 33(1), January 1997.

[13] Y. F. Chen, Y. P. Lan, and H. L. Chang. Analytical model for design criteria of passively Q-switched lasers. *IEEE Journal of Quantum Electronics*, 37(3), March 2001.

[14] F. Patel and R. Beach. New formalism for the analysis of passively Q-switched laser systems. *IEEE Journal of Quantum Electronics*, 37(5), May 2001.

[15] X. Zhang, S. Zhao, Q. Wang, B. Ozygus, and H. Weber. Modeling of passively Q-switched lasers. *Journal of the Optical Society of America B*, 17(7), July 2000.

[16] G. Xiao and M. Bass. Additional experimental confirmation of the predictions of a model to optimize passively Q-switched lasers. *IEEE Journal of Quantum Electronics*, 34(7):1142–1143, July 1998.

[17] W. Koechner and M. Bass. *Solid-State Lasers*. Springer-Verlag, 2003.

[18] A. E. Siegman. *Lasers*. University Science Books, 1986.

REFERENCES

[19] J. T. Verdeyen. *Laser Electronics*. Prentice Hall, Upper Saddle River, NJ, 3rd edition, 2000.

[20] F. L. Pedrotti and L. S. Pedrotti. *Introduction to Optics*. Prentice Hall, Upper Saddle River, NJ, 2nd edition, 1993.

[21] J. B. Khurgin, F. Jin, G. Solyar, C. Wmg, and S. Trivedi. Timing jitter reduction in diode pumped passively Q-switched laser with composite pumping pulses. *CLEO*, 2001.

[22] P. Yan, X. Tian, M. Gong, and T. Xie. Laser performance of monolithic Cr, Nd:YAG crystal with prepumping modulation. *Optical Engineering*, 44(1), January 2005.

[23] D.G. Grant. A technique for obtaining single, high peak power pulses from a ruby laser. *Proceedings of the IEEE*, 51(4):604, April 1963.

[24] J. I. Masters, J. Ward, and E. Hartouni. Laser Q-spoiling using an exploding film. *Review of Scientific Instruments*, 34(4):365–367, April 1963.

[25] E. Reed. A flashlamp-pumped, Q-switched Cr:Nd:GSGG laser. *IEEE Journal of Quantum Electronics*, 21(10), October 1985.

[26] J. A. Caird, M. D. Shinn, T. A. Kirchoff, L. K. Smith, and R. E. Wilder. Measurements of losses and lasing efficiency in GSGG:Cr,Nd and YAG:Nd laser rods. *Applied Optics*, 25(23):4294–4305, December 1986.

[27] V. G. Ostroumov, Y. S. Privis, V. A. Smirnov, and I. A. Shcherbakov. Sensitizing of Nd^{3+} luminescence by Cr^{3+} in gallium garnets. *Journal of the Optical Society of America B*, 3(1), January 1986.

[28] W. F. Krupke, M. D. Shinn, J. E. Marion, J. A. Caird, and S. E. Stokowski. Spectroscopic, optical, and thermomechanical properties of neodymium- and

REFERENCES

chromium-doped gadolinium scandium gallium garnet. *Journal of the Optical Society of America B*, 3(1), January 1986.

[29] E. V. Zharikov, I. I. Kuratev, V. V. Laptev, S. P. Nasel'skee, A. I. Ryabove, G. N. Toropkin, A. V. Shestakov, and I. A. Shcherbakov. Effect of uv- and γ-irradiation on the lasing characteristics of neodymium lasers. *Bulletin of the Academy of Sciences of the USSR*, 48(7):103–105, 1984.

[30] D. P. Caffey and R. A. Utano. Diode array side-pumped neodymium-doped gadolinium scandium gallium garnet rod and slab lasers. *Applied Physics Letters*, 56(9), February 1990.

[31] W. Koechner. *Solid-State Laser Engineering.* Springer-Verlag, 5th edition, 1999.

[32] I. J. Miller, A. J. Alcock, and J. E. Bernard. Experimental investigation of Cr^{4+} in YAG as passive Q-switch. *OSA Proceedings on Advanced Solid-State Lasers*, 13, 1992.

[33] Y. Shimony, Y. Kalisky, and B. H. T. Chai. Quantitative studies of Cr^{4+}:YAG as a saturable absorber for Nd:YAG laser. *Optical Materials*, March 1995.

[34] Y. Shimony, Z. Burshtein, and Y. Kalisky. Cr^{4+}:YAG as passive Q-switch and brewster plate in a pulsed Nd:YAG laser. *IEEE Journal of Quantum Electronics*, 31(10), October 1995.

[35] Y. Y. Kalisky, A. Ben-Amar Baranga, Y. Shimony, Z. Burshtein, S. A. Pollack, and M. R. Kokta. Cr^{4+} doped garnets: their properties as non-linear absorbers. *Optical Materials*, November 1996.

[36] G. Xiao, J. H. Lim, S. Yang, E. Van Stryland, M. Bass, and L. Weichman. Z-scan measurement of the ground and excited state absorption cross sections of Cr^{4+} in yttrium aluminum garnet. *IEEE Journal of Quantum Electronics*, 35(7):1086–1091, July 1999.

REFERENCES

[37] J. Chen, H. Kung, H. Yau, H. Liu, T. Chen, and C. Cheng. Passive Q-switches for Nd:hosted solid state lasers. *Optical Review*, 7(6):511–519, November 2000.

[38] B. Lipavsky, Y. Kalisky, Z. Burshtein, Y. Shimony, and S. Rotman. Some optical properties of Cr^{4+}-doped crystals. *Optical Materials*, 13(1):117–127, October 1999.

[39] Z. Burshtein, P. Blau, Y. Kalisky, Y. Shimony, and M. R. Kikta. Excited-state absorption studies of Cr^{4+} ions in several garnet host crystals. *IEEE Journal of Quantum Electronics*, 34(2):292–299, February 1998.

[40] H. Eilers, K. R. Hoffman, W. M. Dennis, S. M. Jacobsen, and W. M. Yen. Saturation of 1.064 micron absorption in $Cr,Ca:Y_3Al_5O_{12}$ crystals. *Applied Physics Letters*, 61(25):2958–2960, December 1992.

[41] H. Eilers, U. Hömmerich, S. M. Jacobsen, W. M. Yen, K. R. Hoffman, and W. Jia. Spectroscopy and dynamics of $Cr^{4+}:Y_3Al_5O_{12}$. *Phys. Rev. B*, 49(22):15505–15513, June 1994.

[42] A. Sennaroglu, C. R. Pollock, and H. Nathel. Efficient continuous-wave chromium-doped YAG laser. *Journal of the Optical Society of America B*, 12(5), 1995.

[43] M. Hercher. An analysis of saturable absorbers. *Applied Optics*, 6(5), May 1967.

[44] H. Liu, S. Zhou, and Y. C. Chen. High-power monolithic unstable-resonator solid-state laser. *Optics Letters*, 23(6), March 1998.